nature cell biology

ARTICLES

https://doi.org/10.1038/s41556-020-00592-8

Check for updates

PLCγ1 suppression promotes the adaptation of KRAS-mutant lung adenocarcinomas to hypoxia

Maria Saliakoura[1], Matteo Rossi Sebastiano[1,8], Chiara Pozzato[1,8], Florian H. Heidel[2,3], Tina M. Schnöder[2,3], Spasenija Savic Prince[4], Lukas Bubendorf[4], Paolo Pinton[5], Ralph A. Schmid[6], Johanna Baumgartner[7], Stefan Freigang[7], Sabina A. Berezowska[7], Alessandro Rimessi[5] and Georgia Konstantinidou[1]✉

Mutant KRAS modulates the metabolic plasticity of cancer cells to confer a growth advantage during hypoxia, but the molecular underpinnings are largely unknown. Using a lipidomic screen, we found that PLCγ1 is suppressed during hypoxia in KRAS-mutant human lung adenocarcinoma cancer cell lines. Suppression of PLCγ1 in hypoxia promotes a less oxidative cancer cell metabolism state, reduces the formation of mitochondrial reactive oxygen species and switches tumour bioenergetics towards glycolysis by impairing Ca^{2+} entry into the mitochondria. This event prevents lipid peroxidation, antagonizes apoptosis and increases cancer cell proliferation. Accordingly, loss of function of *Plcg1* in a mouse model of $Kras^{G12D}$-driven lung adenocarcinoma increased the expression of glycolytic genes, boosted tumour growth and reduced survival. In patients with KRAS-mutant lung adenocarcinomas, low PLCγ1 expression correlates with increased expression of hypoxia markers and predicts poor patient survival. Thus, our work reveals a mechanism of cancer cell adaptation to hypoxia with potential therapeutic value.

Hypoxia is a common feature of solid tumours[1,2] and it is associated with cancer aggressiveness, treatment resistance and poor prognosis[3]. Thus, understanding the mechanisms underlying the adaptation of cancer cells to hypoxia may pave the way to uncover new cancer target requirements for better therapeutic approaches.

Hypoxia can lead to profound rearrangements in cancer lipid metabolism, including inhibition of fatty acid oxidation (FAO), accumulation of triglycerides in lipid droplets (LDs) and alteration of cellular lipid composition by lowering the desaturation index of fatty acids[4–8]. These alterations are potentially important in cancer cell adaptation to hypoxia. For instance, there is evidence indicating that the suppression of FAO during hypoxia shifts the metabolism of cancer cells towards a more glycolytic phenotype, which boosts their survival[7]. Moreover, LDs can have a key role in limiting reactive oxygen species (ROS)-mediated lipid peroxidation during hypoxia by sequestering unsaturated lipids[9,10]. Nevertheless, the identity and contribution of lipid species that are important for cancer cell adaptation to hypoxia are still mostly unknown.

A class of lipids that can ideally mediate cancer signalling adaptations to hypoxia is represented by phosphoinositides[11,12]. There is strong evidence indicating that the interaction between these phospholipid messengers and their binding proteins has key role in cancer cell signalling[13,14]. For example, the level of phosphatidylinositol -3,4,5-trisphosphate ($PI(3,4,5)P_3$) is regulated by PI3K and PTEN, two major signalling nodes in cancer regulation[15]. Furthermore, phosphatidylinositol 4,5-bisphosphate ($PI(4,5)P_2$), another plasma membrane phosphoinositide, attracts PI3K and other phosphoinositide-modifying enzymes, including phospholipase C (PLC). PLC produces inositol triphosphate (IP_3) and diacylglycerol (DAG), both of which are potent second messengers mainly implicated in calcium (Ca^{2+}) signalling and protein kinase C regulation (PKC), respectively, and are involved in signalling functions important for protein and membrane trafficking as well as cytoskeleton organization in response to stimuli[16,17]. Supporting a role of phosphoinositide signalling in the adaptation of cancer cells to hypoxia, there is evidence indicating that PI3K–AKT signalling increases the transcription and translation of hypoxia-inducible factor 1 (HIF1), a crucial orchestrator of cellular adaptation to a low oxygen environment[18,19]. However, the role of other components of the phosphoinositide signalling pathway in the adaptation to hypoxia remains unclear.

Non-small cell lung cancer (NSCLC) constitutes about 85% of all lung malignancies, out of which 30% harbour mutations in *KRAS*. In NSCLC, *KRAS* mutations are associated with aggressive cancers, and the hypoxic phenotype in these tumours is linked to poorer patient survival[20,21]. Here, we set out to unravel the impact of hypoxia on phosphoinositide signalling and its functional implication in KRAS-driven NSCLC.

Results

Hypoxia suppresses PLCγ1 in KRAS-induced lung cancer. To identify a lipid signature that could reflect molecular signalling with a putative relevance in cancer hypoxia, we profiled the changes in phosphoinositide signalling in the A549 human NSCLC cell line, which bears mutated KRAS[22]. We focused our analysis on four phosphoinositide lipids with a key role in membrane signalling propagation: phosphatidylinositol (PI), phosphatidylinositol 4-phosphate (PI4P), $PI(4,5)P_2$ and $PI(3,4,5)P_3$. The shift to hypoxia (1% O_2) did not cause changes in the total amount of PI, PI4P or $PI(4,5)P_2$, but

[1]Institute of Pharmacology, University of Bern, Bern, Switzerland. [2]Internal Medicine II, Hematology and Oncology, University Hospital Jena, Jena, Germany. [3]Leibniz-Institute on Aging, Fritz-Lipmann-Institute, Jena, Jena, Germany. [4]Institute of Pathology, University Hospital Basel, Basel, Switzerland. [5]Department of Medical Sciences, Laboratory for Technologies of Advanced Therapies (LTTA), University of Ferrara, Ferrara, Italy. [6]Department of General Thoracic Surgery, Inselspital, Bern, Switzerland. [7]Institute of Pathology, University of Bern, Bern, Switzerland. [8]These authors contributed equally: Matteo Rossi Sebastiano, Chiara Pozzato. ✉e-mail: georgia.konstantinidou@pki.unibe.ch

resulted in alterations in their total carbon number and fatty acid saturation level (Fig. 1a–d and Extended Data Fig. 1a–c). Among these changes, we found a relative increase in PI4P and PI(4,5)P_2 containing C38:1, C38:2 and C38:3 (Fig. 1a,c,d). The increase in long-chain fatty acids was accompanied by a decrease in saturated C32 and C34 species (Fig. 1a–d). Conversely, we could detect only the most abundant PI(3,4,5)P_3 lipids, C38:3 and C38:4, which appeared significantly reduced in hypoxia (Fig. 1a,e and Extended Data Fig. 1d). Taken together, these data raise the possibility of a perturbation in signalling propagation at the level of PI(4,5)P_2 in hypoxia.

PI(4,5)P_2 is a substrate for both PI3K and PLC (Extended Data Fig. 1e); thus, we sought to understand the impact of hypoxia on these signalling pathways. We focused our analysis on PLCγ1, a PLC isoform that is commonly expressed in lung cancer lesions[23,24]. Immunoblot analysis in two human KRAS-mutant adenocarcinoma cell lines, A549 and H358, and in mouse embryonic fibroblasts (MEFs) generated from a mouse model carrying a Cre-activatable *Kras*^{G12D} allele (*LSL-Kras*^{G12D} in which LSL denotes lox-stop-lox) and a *p53* conditional knockout allele, *p53*$^{flox/flox}$ (*LSL-Kras*$^{G12D/WT}$;*p53*$^{flox/flox}$)[25,26], indicated that while hypoxia led to disparate effects on the phosphorylation status of AKT (pAKT^{Ser473}/AKT, an established readout of PI3K activation[27]) among the cell lines, it consistently caused a similar degree of reduction in both pPLCγ1^{Tyr783} (activated PLCγ1)[28,29] and PLCγ1 protein levels (Fig. 1f). Further analysis showed that *PLCG1* mRNA levels dropped after a shift to hypoxia (Fig. 1g and Extended Data Fig. 1f, black bars). Notably, knockdown of *HIF1A* dampened the suppression of PLCγ1 by hypoxia at the protein level and, at least partially, at the transcriptional level, which suggests that a HIF1α-dependent mechanism is involved (Fig. 1g,h and Extended Data Fig. 1f).

Confocal microscopy experiments in A549 cells showed that in normoxia, both pPLCγ1^{Tyr783} and PLCγ1 colocalize with focal adhesion kinase (FAK)-rich focal contacts at the cell membrane and at perinuclear halos (Fig. 1i). However, 48 h of hypoxia completely and specifically ablated both pPLCγ1^{Tyr783} and PLCγ1 from the cell membrane (Fig. 1i). Of note, it has been shown that the recruitment of PLCγ1 to the cell membrane is critical for the subsequent phosphorylation of tyrosine at position 783 and activation of the enzyme[28,29].

PLCG1 knockdown in A549 cells recapitulated the effect of hypoxia by increasing the relative level of PI(4,5)P_2 containing C38:1, C38:2 and C38:3 species and decreasing the relative level of PI(4,5)P_2 containing C32:0, C34:0 and C36:0 species (Extended Data Fig. 1g,h). Remarkably, *PLCG1* knockdown cooperated with hypoxia to further accumulate C38:1, C38:2 and C38:3 lipid species and suppress C32:0, C34:0 and C36:0 species without affecting the total amount of PI(4,5)P_2 (Extended Data Fig. 1g–i). These results further corroborate the cause–effect relationship between hypoxia and PLCγ1 suppression in NCSLC cells.

To functionally support our results in vivo, we assessed the status of pPLCγ1^{Tyr783} and PLCγ1 in lung tumour tissue derived from *LSL-Kras*$^{G12D/WT}$;*p53*$^{flox/flox}$ mice. To detect the hypoxic lung tumour areas, we injected mice with pimonidazole (hypoxyprobe), a 2-nitroimidazole, and we found positive pPLCγ1^{Tyr783} and PLCγ1 staining in more than 22% and 35% of the nonhypoxic tumour cells, respectively, while only about 10–15% stained positive in hypoxic tumour cells (Fig. 1j).

Altogether, our data indicate that PLCγ1 is suppressed in hypoxic KRAS-mutant lung cancer cells.

PLCγ1 suppression enhances cancer cell survival during hypoxia. Next, we abolished PLCγ1 via doxycycline-inducible RNA-interference-mediated knockdown in A549, H358 and A427 NSCLC cell lines harbouring *KRAS* mutations and assessed proliferation in normoxia or after a shift to hypoxia. In normoxia, *PLCG1* knockdown decreased cancer cell proliferation (Fig. 2a,b and Extended Data Fig. 2a–c). Moreover, the shift from normoxia to hypoxia caused a strong decrease in cancer cell proliferation. Yet, knockdown of *PLCG1* significantly reverted the antiproliferative effect of hypoxia (Fig. 2b and Extended Data Fig. 2b,c). Both the decreased cell proliferation in normoxia and the increased cell proliferation in hypoxia after *PLCG1* knockdown compared with the controls was rescued via the expression of a short-hairpin-RNA-resistant PLCγ1 (shRNA-rPLCγ1; Fig. 2c and Extended Data Fig. 2d). Notably, the overexpression of PLCγ1 in A549 cells bolstered cell proliferation in normoxia while suppressed it in hypoxia (Fig. 2c, shControl empty vector versus shControl + rPLCγ1). Of note, *PLCG1* knockdown did not affect the protein level of other PLC isoenzymes, which suggests that there is a lack of compensatory effects (Extended Data Fig. 2e).

Our results showed a possible association between hypoxia and inhibition of PI3K in A549 cells (Fig. 1f). Treatment of A549 with LY294002 or wortmannin, two PI3K inhibitors, decreased cancer cell proliferation in normoxic conditions (Extended Data Fig. 2f,g). However, neither drug had an impact on cell proliferation in hypoxia, which suggests that the observed change in the PI3K pathway is not relevant in this hypoxic context (Extended Data Fig. 2g).

Flow cytometry assessment revealed an increase in Annexin V and propidium iodide (ANN/PI)-positive A549 cells after *PLCG1* knockdown in normoxia, which indicates that PLCγ1 is required for cell survival in this context (Fig. 2d and Extended Data Fig. 3a). Moreover, the shift from normoxia to hypoxia resulted in about a fourfold increase in cell death. However, *PLCG1* knockdown significantly suppressed hypoxia-induced cell death, and this was rescued

Fig. 1 | Hypoxia alters phosphoinositide fatty acid composition and suppresses PLCγ1. a, Heatmap showing lipid fold-changes (coloured bar) in A549 cells after a shift from normoxia to hypoxia for 48 h as analysed by ultra-performance liquid chromatography–tandem mass spectrometry; $n = 4$ biologically independent samples per group. PI, phosphatidylinositol. **b**–**e**, Detectable peak areas of PI (**b**), PI4P (**c**), PI(4,5)P_2 (**d**) and PI(3,4,5)P_3 (**e**) in A549 cells treated as in **a**; $n = 4$ biologically independent samples per group. Graphs in **b** and **d** are segmented to highlight less abundant lipids. **f**, Immunoblot analysis in A549, H358 and MEFs treated as indicated. MEFs were generated from *LSL-Kras*$^{G12D/WT}$;*p53*$^{flox/flox}$ (*fl*, *flox*) mice and stably transduced with pMSCV-hygro-Cre. **g**, *PLCG1* mRNA expression level in A549 cells (relative to normoxia control at 24 h). Cells were transduced with either an empty vector (Tet-pLKO-puro, shControl) or a doxycycline-inducible shRNA against *HIF1A* (shHIF1α) and incubated in normoxia or hypoxia conditions for the indicated time points; $n = 3$ biologically independent samples. **h**, Immunoblot analysis of A549 cells transduced as in **g** and incubated in normoxia or hypoxia conditions for 48 h. **i**, Representative confocal microscopy images showing immunofluorescence for pPLCγ1^{Tyr783} or PLCγ1 (green) and FAK (red) in A549 cells incubated in normoxia or hypoxia conditions for 48 h. Hoechst staining was used for nuclei. The white arrows mark the magnified areas shown on the right. **j**, Representative confocal microscopy images showing immunofluorescence for pimonidazole (Pimo), pPLCγ1^{Tyr783} or PLCγ1 on lung tumours from *Kras*$^{G12D/WT}$;*p53*$^{flox/flox}$ mice (left), and the percentage of pPLCγ1^{Tyr783} and PLCγ1 occupancy in pimonidazole-negative versus pimonidazole-positive tumour cells (right). $n = 7$ (pPLCγ1^{Tyr783}) or $n = 9$ (PLCγ1) biologically independent replicates per group. Mouse FITC and rabbit FITC anti-pimonidazole were used for pPLCγ1^{Tyr783} and PLCγ1 staining, respectively. White arrowheads show nonhypoxic areas, while orange arrowheads show hypoxic areas. The samples in panels **f** and **h** are derived from the same experiment, and the gels/blots were processed in parallel. Graphical data are shown as the mean ± s.d. Statistical analyses were done using unpaired Student's *t*-test or one-way ANOVA. $^*P < 0.05$, $^{**}P < 0.01$, $^{****}P < 0.0001$. Statistical source data and unprocessed immunoblots are provided in the source data.

via the expression of a shRNA-rPLCγ1 (Fig. 2d and Extended Data Fig. 3a). These results were additionally confirmed with a caspase-3 activity assay (Extended Data Fig. 3b). Intriguingly, Q-VD-OPH, a pan-caspase inhibitor, did not completely rescue hypoxia-induced cell death, which suggests that other cell death mechanisms are implicated in addition to caspase-dependent apoptosis (Extended Data Fig. 3c). Last, we found that overexpression of PLCγ1 in hypoxia caused a 2.5-fold increase in cell death (Extended Data Fig. 3d).

Next, to assess the effects of PLCγ1 suppression in a genetically defined model, we generated MEFs from a combined Cre-activatable *Kras*$^{G12D/WT}$ and conditional *p53*$^{flox/flox}$ alleles (*LSL-Kras*$^{G12D/WT}$;*p53*$^{flox/flox}$) that were wild type (*Plcg1*$^{wt/wt}$), heterozygous (*Plcg1*$^{wt/flox}$) or homozygous for a Cre-conditional *Plcg1* allele (*Plcg1*$^{flox/flox}$), hereafter named *Kras*^{G12D};*Plcγ1*$^{+/+}$, *Kras*^{G12D};*Plcg1*$^{+/-}$ and *Kras*^{G12D};*Plcg1*$^{-/-}$, respectively. Subsequently, we transduced these MEFs with a Cre-expressing lentiviral construct to concomitantly turn on

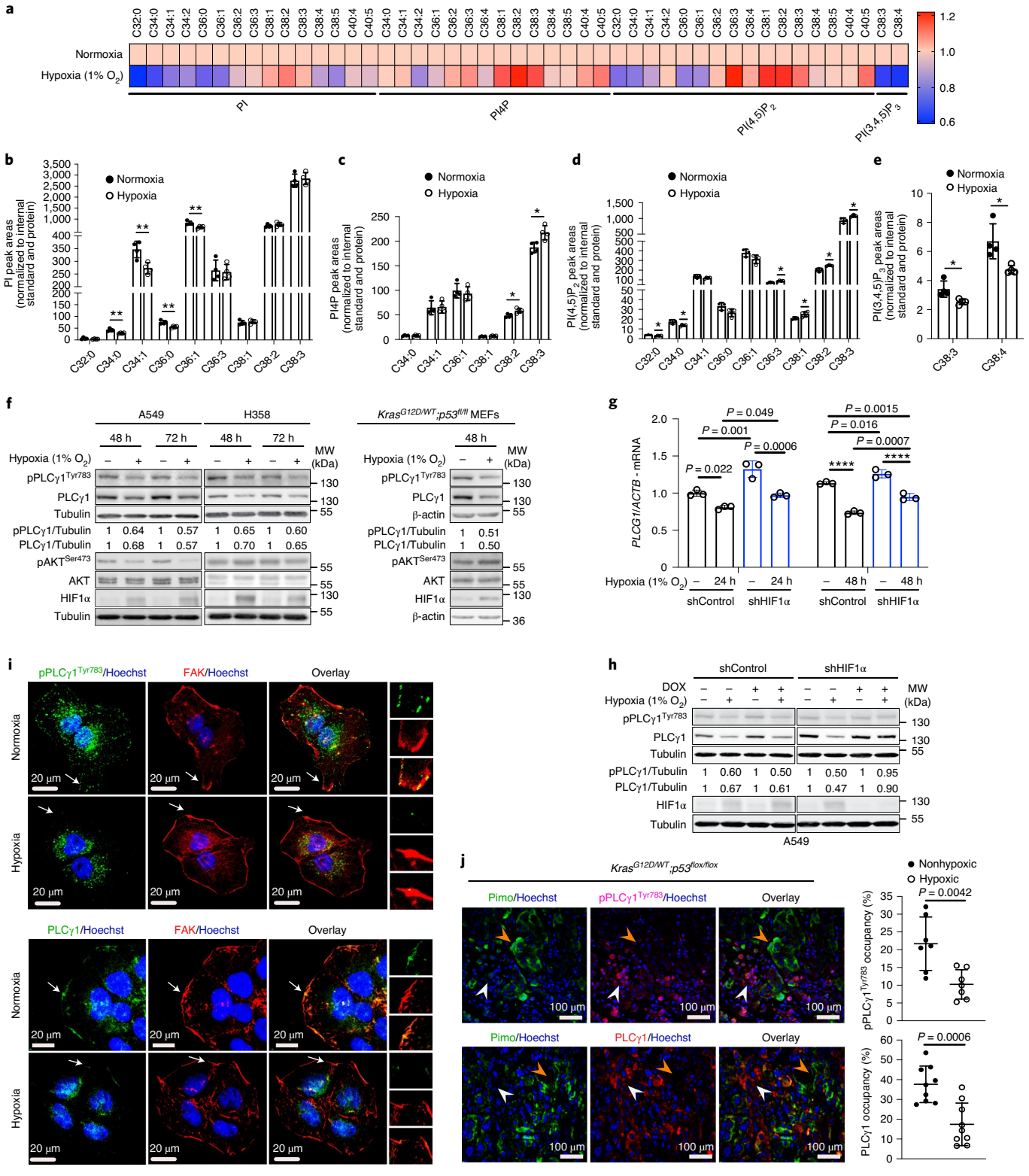

Kras^{G12D} and knockout *p53* and *Plcg1* (Fig. 2e). We found that in normoxia, the *Kras*^{G12D};*Plcg1*$^{+/-}$ and *Kras*^{G12D};*Plcg1*$^{-/-}$ cells showed decreased proliferation and increased cell death compared with the *Kras*^{G12D};*Plcg1*$^{+/+}$ cells (Fig. 2f,g and Extended Data Fig. 3e,f). However, in hypoxia, the *Kras*^{G12D};*Plcg1*$^{+/-}$ and *Kras*^{G12D};*Plcg1*$^{-/-}$ cells exhibited enhanced proliferation and decreased cell death compared with the hypoxic *Kras*^{G12D};*Plcg1*$^{+/+}$ cells, thereby confirming the results obtained with the human A549 cells (Fig. 2f,g and Extended Data Fig. 3e,f). Next, we injected the *Kras*^{G12D};*Plcg1*$^{+/+}$, *Kras*^{G12D};*Plcg1*$^{+/-}$ and *Kras*^{G12D};*Plcg1*$^{-/-}$ cell lines subcutaneously in immunocompromised mice to assess tumour formation in vivo. We found that either partial (*Kras*^{G12D};*Plcg1*$^{+/-}$) or complete suppression of PLCγ1 (*Kras*^{G12D};*Plcg1*$^{-/-}$) resulted in increased tumour burden and decreased survival of mice compared with the mice injected with the *Kras*^{G12D};*Plcg1*$^{+/+}$ cells (Fig. 2h,i). The increased tumour burden was due to increased proliferation and decreased apoptosis, as shown by the percentage of Ki67-positive and Tunel-positive cells, respectively (Fig. 2j–l). These data suggest that either heterozygous or homozygous deletion of *Plcg1* provides a survival advantage over the hypoxic control cells.

Taken together, these results indicate that the suppression of PLCγ1 hinders the proliferation and survival of lung cancer cells in normoxia, whereas it circumvents hypoxia-induced stress by promoting their proliferation and survival.

PLCγ1 suppression reduces mitochondrial oxidative metabolism and enhances the glycolytic capacity of cancer cells. Ca^{2+} regulates mitochondrial oxidative phosphorylation (OXPHOS), therefore contributing to the maintenance of cellular energy homeostasis and viability[30–32]. PLCγ1, by producing IP_3, triggers Ca^{2+} mobilization from the endoplasmatic reticulum (ER) to regulate mitochondrial functionality[33–35]. *PLCG1* knockdown in A549 cells reduced the rate of histamine-induced Ca^{2+} release from the ER without altering the luminal ER Ca^{2+} concentration at rest (Fig. 3a). This resulted in a decreased cytosolic and mitochondrial Ca^{2+} response in *PLCG1* knocked down cells compared with control cells, thereby confirming that *PLCG1* silencing triggers a sharp functional effect. To assess mitochondrial function, we measured the mitochondrial oxygen consumption rate (OCR), a marker of mitochondrial respiratory capacity and energy production, in A549 cells. We found that in normoxia, *PLCG1* knockdown did not have an impact on basal respiration or mitochondrial ATP production, but the maximal respiration and spare respiratory capacity were significantly lower than in control cells. This suggests that there is mild mitochondrial dysfunction that is not apparent under basal conditions, but becomes evident only under increased ATP demand (Fig. 3b and Extended Data Fig. 4a–c). However, in hypoxia, we observed an overall reduction in all the OCR parameters after *PLCG1* knockdown, which suggests that the cells are unable to maintain an adequate level of mitochondrial respiration (Fig. 3b and Extended Data Fig. 4a–c). The extent of the metabolic difference between *PLCG1* knockdown in normoxia and hypoxia was evident by the increased extracellular acidification rate (ECAR), which indicates the rate of glycolysis. Indeed, under basal conditions (unstimulated), glycolysis remained unaltered in normoxia while it increased in hypoxia after PLCγ1 knockdown, which suggests that there is a metabolic switch from OXPHOS to aerobic glycolysis (Fig. 3c and Extended Data Fig. 4d,e). Importantly, the increased glycolysis after *PLCG1* knockdown in hypoxia was rescued via the expression of a shRNA-rPLCγ1 (Extended Data Fig. 4f). Furthermore, overexpression of PLCγ1 increased the OCR in both normoxia and hypoxia (Extended Data Fig. 4g) and decreased glycolysis in hypoxia (Fig. 3d and Extended Data Fig. 4h). Last, we found that the *Kras*^{G12D};*Plcg1*$^{+/-}$ and *Kras*^{G12D};*Plcg1*$^{-/-}$ MEFs had decreased OCRs and enhanced glycolysis compared with the *Kras*^{G12D};*Plcg1*$^{+/+}$ control cells in hypoxia (Fig. 3e and Extended Data Fig. 5a–c). Notably, the enhanced glycolysis of *Kras*^{G12D};*Plcg1*$^{+/-}$ and *Kras*^{G12D};*Plcg1*$^{-/-}$ MEFs in hypoxia was rescued by PLCγ1 overexpression (Fig. 3e and Extended Data Fig. 5a–c).

Our results suggest that *PLCG1* knockdown impairs mitochondrial oxidative metabolism that could result in decreased mitochondrial capacity to oxidize lipids. Indeed, FAO decreased after *PLCG1* knockdown in hypoxia, an effect that was rescued via the expression of a shRNA-rPLCγ1 (Fig. 3f). Moreover, PLCγ1 overexpression enhanced FAO both in normoxia and hypoxia (Fig. 3g). Since triacylglycerols (TAGs) are a source of fatty acids for mitochondrial FAO, we quantified the total amount of TAGs after *PLCG1* knockdown. Intriguingly, *PLCG1* knockdown resulted in a major increase in TAGs in both normoxia and hypoxia (Fig. 3h). Staining of LDs with LipidTOX, a LD marker, and measurement by flow cytometry analysis showed that *PLCG1* knockdown results in a significant increase in LDs (Fig. 3i and Extended Data Fig. 5d). Confocal microscopy revealed that this was due to an increase in the LD size after *PLCG1* knockdown (Fig. 3j,k). The accumulation of LDs after FAO inhibition was recapitulated via the treatment of A549 cells with etomoxir, a FAO inhibitor, which suggests that TAG accumulation is due to the reduced mitochondrial capacity to oxidize lipids (Fig. 3l). These results indicate that PLCγ1 inhibition impairs fatty acid catabolism accumulating TAGs in LDs.

Overall, our data suggest that PLCγ1 inhibition mediates a more efficient metabolic reprogramming effect, thereby improving the adaptation of mutant KRAS cancer cells to hypoxia.

PLCγ1 suppression mediates the adaptation of cancer cells to hypoxia by reducing ROS. Experimental evidence supports the possibility that exposure of cells to hypoxia, including lung cancer cells, increases ROS production[36,37]. Indeed, we found that ROS levels increased by about twofold in A549 cells after a shift from normoxia to hypoxia (Fig. 4a and Extended Data Fig. 6a). Nevertheless,

Fig. 2 | PLCγ1 suppression promotes cancer cell survival during hypoxia. a, Immunoblot analysis of A549 cells transduced with either an empty vector (Tet-pLKO-pur;, shControl) or two doxycycline-inducible shRNAs against *PLCG1* (shPLCγ1-1 and shPLCγ1-2) and incubated without or with doxycycline (DOX) for 72 h. **b**, The relative cell number of A549 cells transduced as in **a** and incubated in normoxia or hypoxia conditions for the indicated time points; $n=3$. **c**, The relative cell number of A549 cells transduced as in **a**. After 24 h, cells were transfected with either pcDNA3.1 empty vector or pcDNA3.1-rPLCγ1: shPLCγ1-2 + rPLCγ1 and further incubated in normoxia (left) or hypoxia (right) conditions for the indicated time points; $n=3$. Normoxia: $^{***}P=0.0005$, hypoxia: $^{**}P=0.0033$, $^{***}P=0.0006$. **d**, Representative panels of Ann–Atto 633/PI flow cytometry analysis (left) and relative quantification of Ann + Ann/PI-positive A549 cells (right) treated as in **c**; $n=3$. **e**, Immunoblot analysis of MEFs generated from mice of the indicated genotypes and stably transduced with pMSCV-hygro-Cre recombinase where indicated. **f**, The relative cell number of MEFs transduced as in **e** and treated as indicated; $n=3$. $^{**}P=0.0021$, $^{***}P=0.0008$. **g**, Ann + Ann/PI-positive cell quantification by flow cytometry in MEFs transduced as in **e**, incubated in normoxia or hypoxia conditions and analysed by flow cytometry; $n=3$. $^{**}P=0.0042$. **h**,**i**, Tumour burden quantification (**h**) and overall survival (**i**) of immunocompromised mice. MEFs were transduced as in **e** and subcutaneously injected into mice; $n=5$ mice per group (*Kras*^{G12D};*Plcg1*$^{+/+}$, $n=4$ mice). **j–l**, Representative images of Ki67 IHC (**j**, top), Tunel assay (**j**, bottom) and related quantifications (**k** and **l**) from tumours generated as in **h**; $n=4$ mice per group, *Kras*^{G12D};*Plcg1*$^{+/-}$ (**l**) $n=5$ mice. In **j**, the arrowheads indicate Tunel-positive cells shown at higher magnification in the inset. Graphical data are shown as the mean ± s.d. Statistical analyses were done using one-way ANOVA or log-rank (Mantel–Cox) test (where indicated). The *n* in panels **b–d, f** and **g** refers to biologically independent samples/group. $^{****}P<0.0001$. Statistical source data and unprocessed immunoblots are provided in the source data.

PLCG1 knockdown significantly suppressed ROS production in hypoxia, which was rescued via the expression of a shRNA-rPLCγ1 (Fig. 4a and Extended Data Fig. 6a). *PLCG1* knockdown also caused a moderate ROS increase in normoxia, which was rescued via the expression of a shRNA-rPLCγ1 (Fig. 4a). Moreover, overexpression of PLCγ1 in hypoxia intensified ROS levels, thereby additionally supporting a role of PLCγ1 in modulating ROS production (Fig. 4b). Notably, treatment with the mitochondria-targeted antioxidant mitoTEMPO suppressed hypoxia-induced ROS in A549 cells, thus indicating a mitochondrial source of ROS (Fig. 4c).

Ca^{2+} stimulates activity of the electron transport chain, which influences mitochondrial ROS production during hypoxia[38]. Thus, we investigated whether PLCγ1 controls ROS production through the regulation of Ca^{2+} mobilization to mitochondria. First, we silenced the mitochondrial calcium uniporter (MCU), the machinery responsible for Ca^{2+} uptake into the matrix[39,40], and assessed

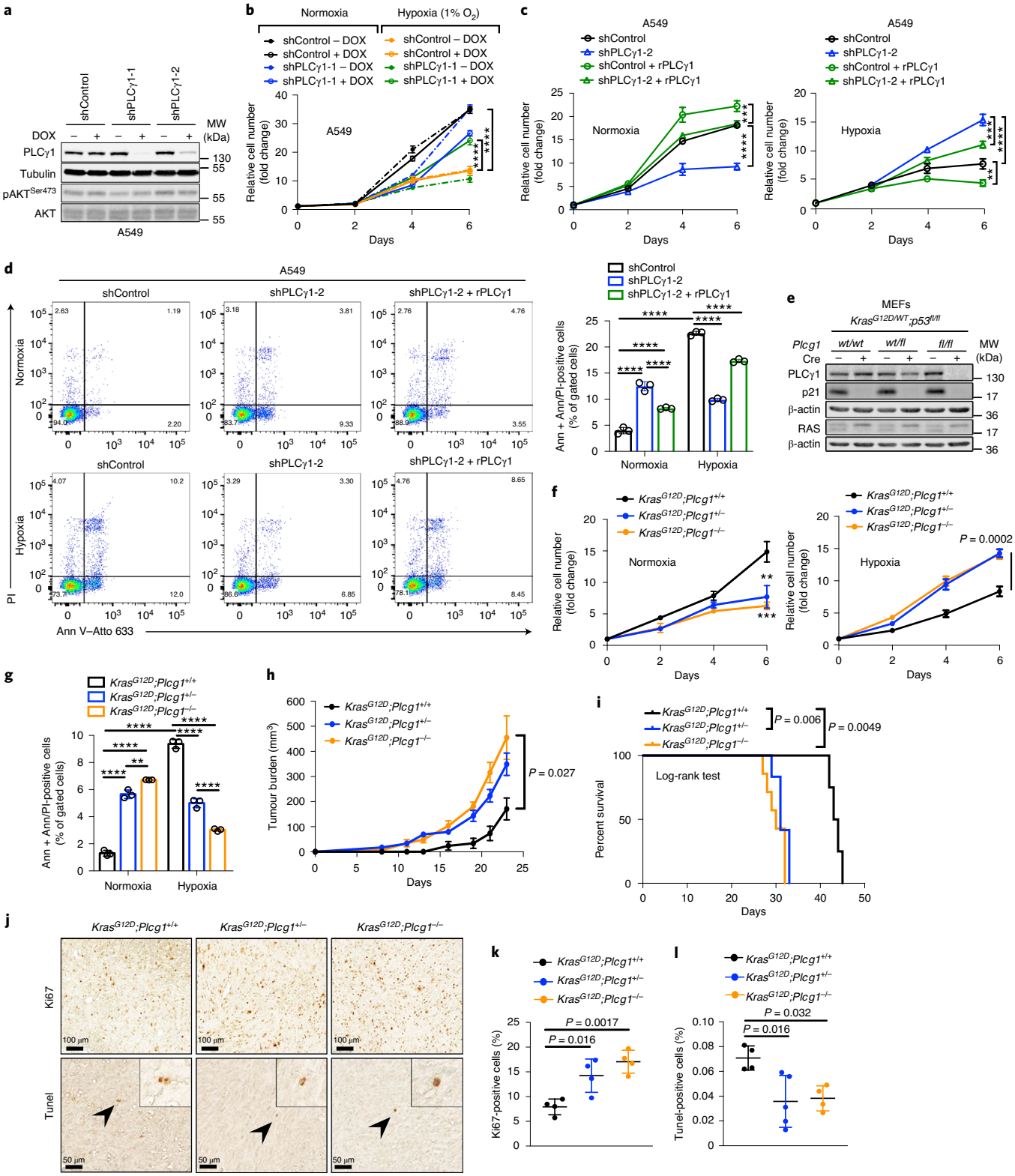

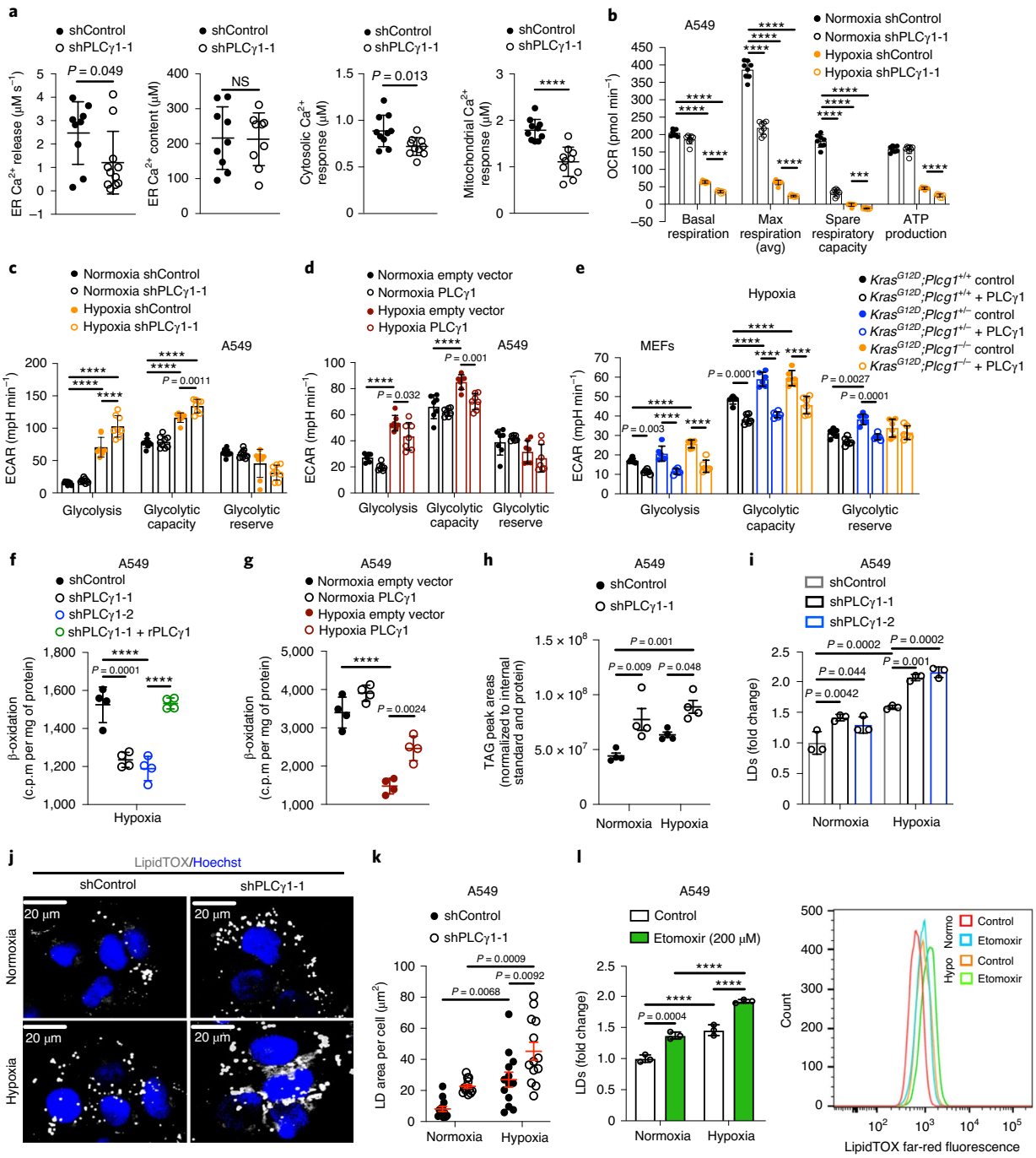

Fig. 3 | PLCγ1 suppression decreases mitochondrial respiration and enhances cancer cell glycolytic capacity. a, ER Ca^{2+} release rate ($n = 9/11$), intraluminal content ($n = 9$), cytosolic and mitochondrial Ca^{2+} response ($n = 10$) in cells transduced with either empty vector (shControl) or doxycycline-inducible shRNA against *PLCG1*. NS, not significant. **b**, OCR in A549 cells transduced as in **a**, incubated with doxycycline for 48 h and moved to normoxia or hypoxia conditions for 48 h; $n = 8$. Avg, average. **c**, ECAR in A549 cells transduced and treated as in **b**; *n* (normoxia/hypoxia) = 9/8. **d**, ECAR in A549 cells transfected with either pcDNA3.1 empty vector or pcDNA3.1-PLCγ1 and incubated for 48 h in normoxia or hypoxia conditions; $n = 7$. **e**, ECAR in MEFs of the indicated genotype transfected with either pcDNA3.1-HA-LIC empty vector (control) or pcDNA3.1-HA-LIC-PLCγ1 and incubated for 48 h in hypoxia; $n = 6$. **f**, β-oxidation of cells transduced with either an empty vector (shControl) or doxycycline-inducible shRNAs against *PLCG1*, transfected with pcDNA3.1 empty vector or pcDNA3.1-rPLCγ1 (rPLCγ1) and incubated for 48 h in hypoxia; $n = 4$. **g**, β-oxidation of cells transfected with either pcDNA3.1 empty vector or pcDNA3.1-PLCγ1 and incubated for 48 h in normoxia or hypoxia; $n = 4$. **h**, TAGs measured by ultra-performance liquid chromatography–tandem mass spectrometry of cells treated as in **b**; $n = 4$ per group. **i**, LD quantification by flow cytometry (relative to normoxia) of cells transduced as in **b** and stained with LipidTOX (far red); $n = 3$ **j**, Representative confocal fluorescence microscopy images of LD staining with LipidTOX (far red) in cells treated as in **b**. **k**, Representative quantification of LD area per cell from **j**; $n = 13$ biologically independent replicates (50 cells per replicate). **l**, LD quantification (relative to normoxia; Normo) by flow cytometry (left) and representative flow cytometry panel (right) of cells treated as indicated and stained with LipidTOX; $n = 3$. Hypo, hypoxia. Graphical data are shown as the mean ± s.d. Statistical analyses were done using two-tailed unpaired Student's *t*-test or one-way ANOVA; *n*, number of biologically independent samples. ****$P < 0.0001$. Statistical source data are provided in the source data.

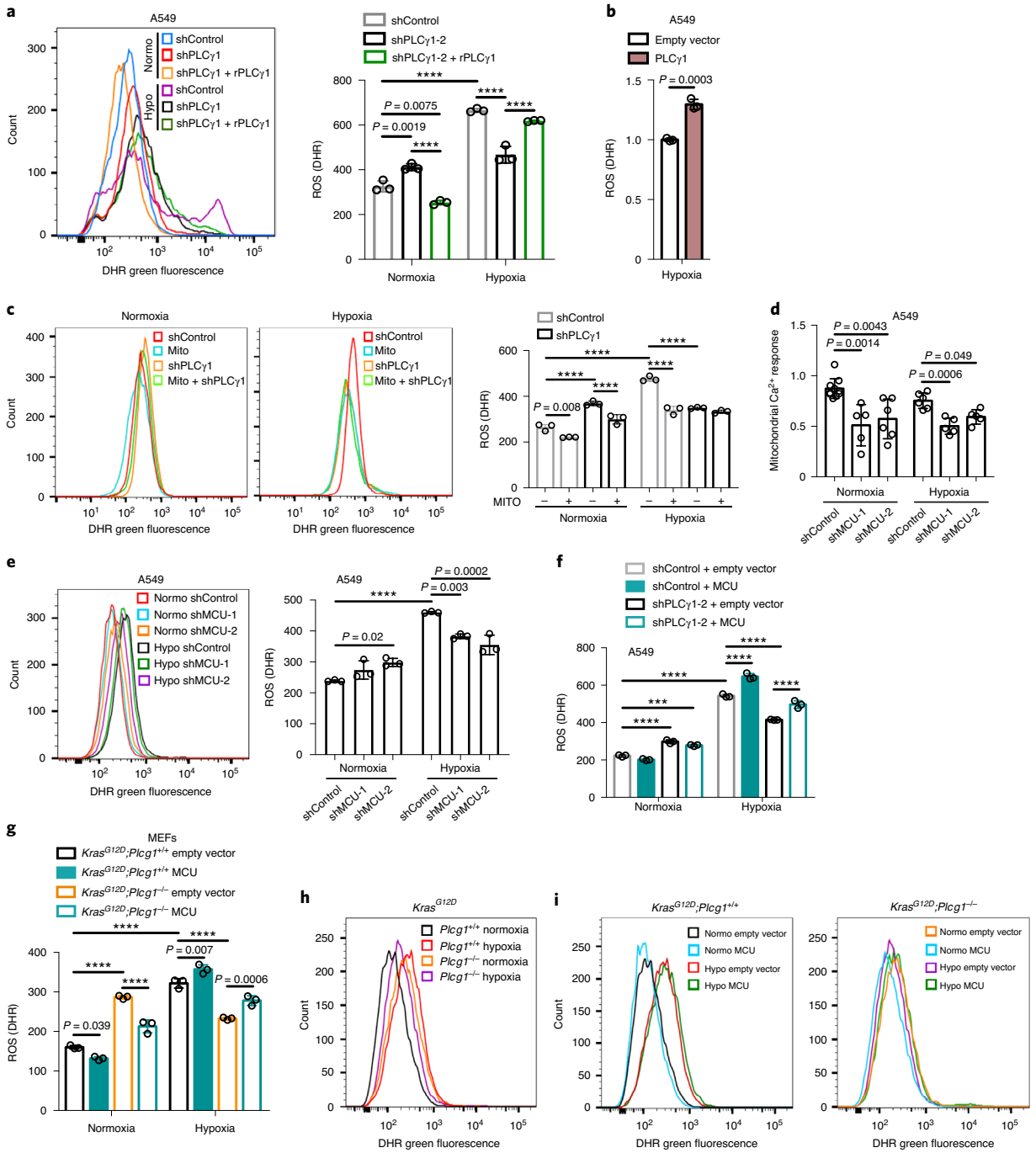

Fig. 4 | PLCγ1 suppression depletes mitochondrial ROS through impairment of Ca^{2+} entry into mitochondria. a, Representative flow cytometry histogram (left) and quantification of DHR (ROS marker, green) (right) of A549 cells transduced with either an empty vector (Tet-pLKO-puro, shControl) or a doxycycline-inducible shRNA against *PLCG1*. Cells were then transfected with either pcDNA3.1 empty vector or pcDNA3.1-rPLCγ1: shPLCγ1-2 + rPLCγ1 and incubated in normoxia or hypoxia conditions for 48 h. $n = 3$. **b**, Flow cytometry quantification of DHR (green) in A549 cells (relative to control) transfected with either pcDNA3.1 empty vector or pcDNA3.1-PLCγ1 and moved to hypoxia conditions for 48 h. $n = 3$. **c**, Representative flow cytometry histograms (left) and quantification of DHR (green, right) of A549 cells transduced and treated as in **a**. At 18 h before staining with DHR for analysis, cells were treated with 10 μM MitoTEMPO (Mito). $n = 3$. **d**, Mitochondrial Ca^{2+} response of A549 cells transduced with an empty vector (Tet-pLKO-puro, shControl) or two doxycycline-inducible shRNAs against *MCU* (shMCU-1 and shMCU-2). Cells were then treated with doxycycline for 24 h, transfected with appropriate targeted aequorin probe and histamine-induced Ca^{2+} measurements were performed after 48 h of incubation in normoxia or hypoxia; *n* per group (left to right) = 9, 5, 6, 6, 5 and 5. **e**, Representative flow cytometry histogram (left) and quantification of DHR (green, right) of A549 cells treated as in **d**. $n = 3$. **f**, Flow cytometry quantification of DHR (green) of A549 cells transduced as in **a**. Cells were then transfected with either pcDNA3.1 empty vector or pcDNA3.1-MCU-Flag plasmid and incubated in normoxia or hypoxia conditions for 48 h. $n = 3$. **g–i**, Flow cytometry quantification (**g**) and representative histograms (**h** and **i**) of DHR (green) in MEFs of the indicated genotype. MEFs were transfected with either pcDNA3.1 empty vector or pcDNA3.1-MCU-Flag plasmid and incubated in normoxia or hypoxia conditions for 48 h. $n = 3$.Graphical data are shown as the mean ± s.d. Statistical analyses were done using two-tailed unpaired Student's *t*-test or one-way ANOVA; *n*, number of biologically independent samples. $^{****}P < 0.0001$. Statistical source data are provided in the source data.

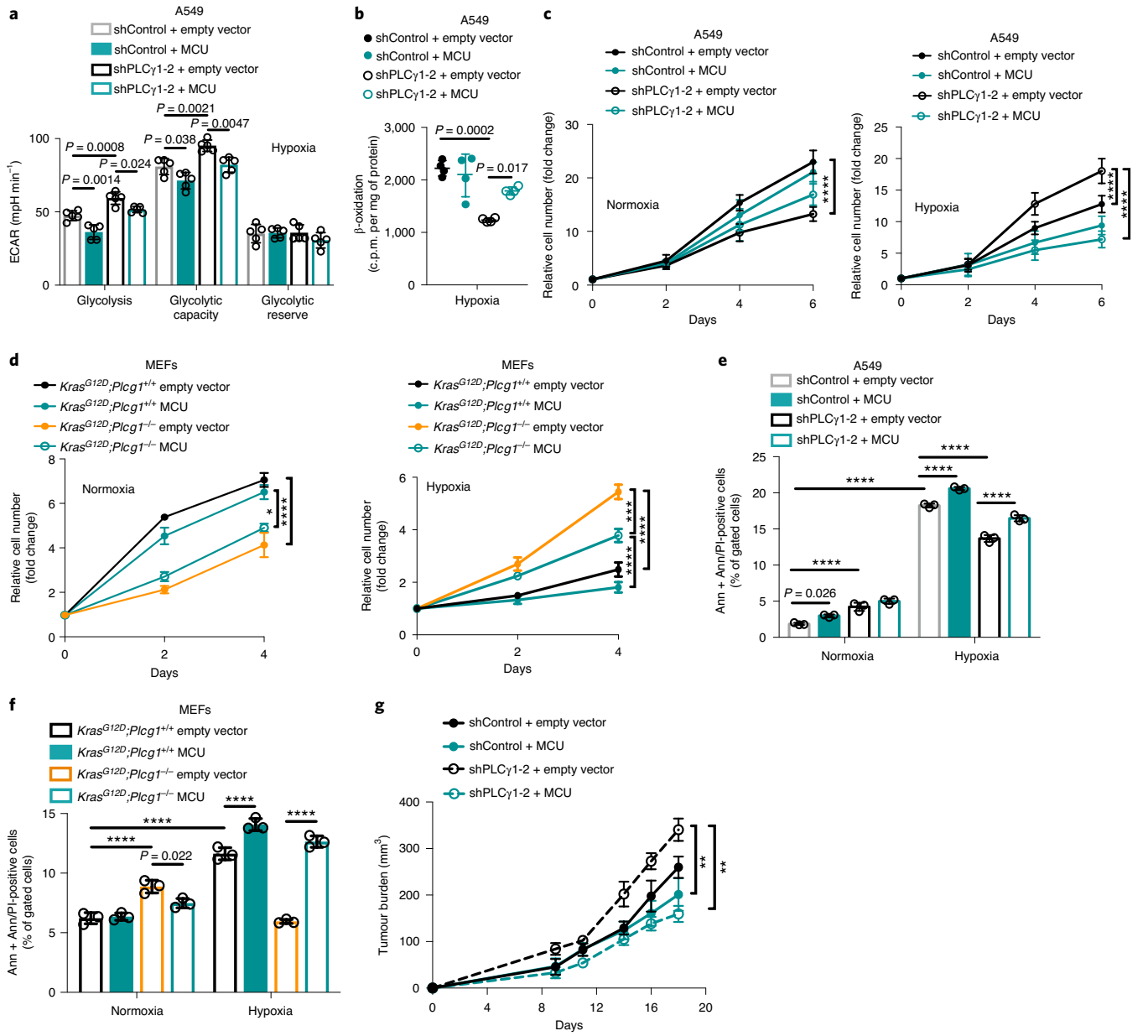

Fig. 5 | Ca^{2+} entry into mitochondria prevents the glycolytic shift and impairs the survival of cancer cells to hypoxia. a, Bar graph showing the ECAR and the different parameters in A549 cells transduced with either an empty vector (Tet-pLKO-puro, shControl) or a doxycycline-inducible shRNA against *PLCG1* (shPLCγ1-2). Cells were then incubated with doxycycline, transfected with either pcDNA3.1 empty vector or pcDNA3.1-MCU–Flag plasmid and incubated in normoxia or hypoxia conditions for 48 h; $n=5$. **b**, Fatty acid β-oxidation of A549 cells in hypoxia treated as in **a**; $n=4$. **c**, The relative cell number of A549 cells in normoxia (left) or hypoxia (right) treated as in **a**; $n=3$. **d**, The relative cell number of the indicated MEFs transfected with either pcDNA3.1 empty vector or pcDNA3.1-MCU–Flag plasmid and incubated in normoxia or hypoxia; $n=3$. $^{*}P=0.022$, $^{***}P=0.0002$. **e**, Ann + Ann/PI-positive cell quantification by flow cytometry analysis in A549 cells treated as in **a** and incubated in normoxia or hypoxia conditions for 72 h. The related panels are reported in Extended Data Fig. 7f; $n=3$. **f**, Ann + Ann/PI-positive cell quantification by flow cytometry analysis in the indicated MEFs transfected with either pcDNA3.1 empty vector or pcDNA3.1-MCU–Flag plasmid and incubated in normoxia or hypoxia. The related panels are reported in Extended Data Fig. 7g; $n=3$. **g**, Tumour burden quantification of A549 cells grown as xenografts in immunocompromised mice. A549 cells were transduced with either pWZL-Hygro empty vector or pWZL-Hygro-MCU–Flag and either with an empty vector control (Tet-pLKO-puro, shControl) or a doxycycline-inducible shRNA against *PLCG1* (shPLCγ1-2) and subcutaneously injected into mice. Tumours were measured every 2–3 days with a caliper; $n=4$ mice per group. $^{**}P=0.0012$. Graphical data are shown as the mean ± s.d. Statistical analyses were done using one-way ANOVA; *n* (**a**–**f**), number of biologically independent samples. $^{****}P<0.0001$. Statistical source data are provided in the source data.

ROS production in normoxia and hypoxia after *PLCG1* knockdown. *MCU* silencing with shRNAs suppressed mitochondrial Ca^{2+} and decreased ROS formation in A549 cells during hypoxia (Fig. 4d,e and Extended Data Fig. 6b). Conversely, MCU overexpression after *PLCG1* knockdown increased ROS production to a level similar to the hypoxic control (Fig. 4f and Extended Data Fig. 6c–f). The effect of PLCγ1 suppression on ROS production was also recapitulated in MEFs. Indeed, $Kras^{G12D};Plcg1^{-/-}$ MEFs generated less ROS in hypoxia compared with $Kras^{G12D};Plcg1^{+/+}$ MEFs, an effect that was rescued by MCU overexpression (Fig. 4g–i and Extended Data Fig. 7a).

MCU overexpression increased the OCR and decreased glycolysis and glycolytic capacity in both control and *PLCG1* knocked down A549 cells during hypoxia (Fig. 5a and Extended Data Fig. 7b,c). Furthermore, although MCU overexpression did not affect β-oxidation of control A549 cells in hypoxia, it rescued the decreased β-oxidation caused by *PLCG1* knockdown (Fig. 5b and Extended Data Fig. 7d).

MCU overexpression enhanced the proliferation of *PLCG1* knocked down A549 cells and $Kras^{G12D};Plcg1^{-/-}$ MEFs in normoxia, while it completely abolished their enhanced cell proliferation in hypoxia (Fig. 5c,d and Extended Data Fig. 7e). Moreover, although cell death was not affected by MCU overexpression in A549 cells, it was significantly suppressed in $Kras^{G12D};Plcg1^{-/-}$ MEFs in normoxia (Fig. 5e,f and Extended Data Fig. 7f,g). In contrast, MCU overexpression abolished the protection against cell death in *PLCG1* knocked down A549 cells and $Kras^{G12D};Plcg1^{-/-}$ MEFs in hypoxia (Fig. 5e,f and Extended Data Fig. 7f,g). Extending the relevance of these data, we found that MCU overexpression impaired subcutaneous A549 xenograft growth in immunocompromised mice and abolished increased tumour growth of the *PLCG1* knocked down group (Fig. 5g).

These results indicate that PLCγ1 suppression hinders ROS production by reducing ER–mitochondria Ca^{2+} transfer and mitochondrial Ca^{2+} overload, hence, improving cancer cell survival during hypoxia.

PLCγ1 suppression reduces lipid peroxidation during hypoxia. Increased ROS levels in hypoxia is a cause of lipid peroxidation and cellular membrane damage[41]. Thus, we hypothesized that PLCγ1 inhibition, by lowering ROS, can rescue the harmful effects of hypoxia-induced lipid peroxidation. Confocal microscopy analysis in A549 cells after staining with the lipid peroxidation sensor BODIPY 581/591 C11 revealed that hypoxia increased lipid peroxidation by about 10% (Fig. 6a,b, filled black dots, and Extended Data Fig. 8a,b). Strikingly, *PLCG1* knockdown suppressed hypoxia-induced lipid peroxidation, which was rescued via the expression of a shRNA-rPLCγ1 (Fig. 6a,b). Moreover, co-staining with LipidTOX showed increased colocalization of the oxidized lipid fraction with LDs in hypoxia, which was abolished by *PLCG1* knockdown (Extended Data Fig. 8a,c). Taken together, these results suggest that *PLCG1* knockdown decreases lipid peroxidation in hypoxia, therefore preventing cell damage.

To examine whether PLCγ1 affects lipid peroxidation through Ca^{2+} mobilization to the mitochondria, we overexpressed MCU and assessed lipid peroxidation in normoxia and hypoxia after *PLCG1* knockdown. Consistent with the effect of MCU-induced ROS changes, MCU overexpression in hypoxic *PLCG1* knocked down cells increased lipid peroxidation to a level comparable to the control-treated cells (Fig. 6c,d).

Previous evidence suggests that during oxidative stress, LDs sequester and protect unsaturated lipids against lipid peroxidation[10]. Therefore, the accumulation of TAGs in LDs could contribute to the increased survival of cells after *PLCG1* knockdown during hypoxia. However, inhibition of TAG formation with a DGAT1 inhibitor (T863) led to only a mild decrease in proliferation after *PLCG1* knockdown in hypoxia, which suggests that LDs play a marginal role in this context (Extended Data Fig. 8d,e).

***Plcg1* suppression promotes $Kras^{G12D}$-driven lung tumour development in mice.** Our in vitro results suggest that PLCγ1 suppression may confer a survival advantage during tumorigenesis. To this aim, we generated mice carrying a Cre-activatable $Kras^{G12D}$ allele, homozygous for a conditional *p53* knockout allele, and wild-type, heterozygous or homozygous for a conditional *Plcg1* allele, to generate three experimental groups: $Kras^{G12D/WT};p53^{flox/flox};Plcg1^{wt/wt}$, $Kras^{G12D/WT};p53^{flox/flox};Plcg1^{wt/flox}$ and $Kras^{G12D/WT};p53^{flox/flox};Plcg1^{flox/flox}$. Adenovirus-mediated Cre delivery to the lungs results in $Kras^{G12D}$ expression and concomitant *p53* and *Plcg1* deletion. Immunohistochemistry (IHC) staining and immunoblotting against PLCγ1 in dissected lung tumours 10 weeks after Cre delivery (tumour onset) showed efficient PLCγ1 depletion in tumours from $Kras^{G12D/WT};p53^{flox/flox};Plcg1^{flox/flox}$ mice compared with the $Kras^{G12D/WT};p53^{flox/flox};Plcg1^{wt/wt}$ control mice (Fig. 7a,b). Of note, *Plcg1* deletion did not have an impact on AKT activation or on the activation status of RAS in dissected lung tumours from $Kras^{G12D/WT};p53^{flox/flox};Plcg1^{flox/flox}$ or $Kras^{G12D/WT};p53^{flox/flox};Plcg1^{wt/wt}$ mice (Fig. 7b). Tumour burden quantification 10 weeks after tumour onset in $Kras^{G12D/WT};p53^{flox/flox};Plcg1^{wt/flox}$ and $Kras^{G12D/WT};p53^{flox/flox};Plcg1^{flox/flox}$ mice showed a striking increase in lung tumour burden after $Kras^{G12D}$ induction compared with the $Kras^{G12D/WT};p53^{flox/flox};Plcg1^{wt/wt}$ control littermates, which indicates that even partial *Plcg1* suppression is sufficient to confer a tumour cell survival advantage in vivo (Fig. 7c and Extended Data Fig. 9a). The increased tumour burden was due to increased tumour sizes and tumour numbers (Fig. 7d). Indeed, the tumours from $Kras^{G12D/WT};p53^{flox/flox};Plcg1^{wt/flox}$ and $Kras^{G12D/WT};p53^{flox/flox};Plcg1^{flox/flox}$ mice showed increased proliferative capacity and decreased cell death compared with the $Kras^{G12D/WT};p53^{flox/flox};Plcg1^{wt/wt}$ tumours, as assessed by Ki67 and Tunel staining, respectively (Fig. 7e and Extended Data Fig. 9b).

Next, we generated mouse cohorts to compare the survival of $Kras^{G12D/WT};p53^{flox/flox};Plcg1^{wt/wt}$ mice to $Kras^{G12D/WT};p53^{flox/flox};Plcg1^{flox/flox}$ mice. In agreement with the increase in lung tumour growth, the survival rate of the $Kras^{G12D/WT};p53^{flox/flox};Plcg1^{flox/flox}$ mice was significantly reduced compared with $Kras^{G12D/WT};p53^{flox/flox};Plcg1^{wt/wt}$ control mice (Fig. 7f).

Quantitative PCR (qPCR) analysis from dissected lung tumours showed that the expression of glycolysis-related genes such as aldolase c (*Aldoc*), enolase 2 (*Eno2*), glucose transporter type 1 (*Glut1*) and lactate dehydrogenase a (*Ldha*), were significantly higher in

Fig. 6 | PLCγ1 suppression reduces hypoxia-induced lipid peroxidation. a, Representative confocal microscopy images showing oxidized and non-oxidized lipids in A549 cells. A549 cells were transduced with either an empty vector control (Tet-pLKO-puro, shControl) or a doxycycline-inducible shRNA against *PLCG1* (shPLCγ1-2). Cells were then incubated in the presence of doxycycline and transfected with either pcDNA3.1 empty vector or pcDNA3.1-rPLCγ1 (shRNA-rPLCγ1: rPLCγ1) to rescue the shPLCγ1-2. Cells were then incubated for additional 48 h in normoxia or hypoxia (1% O_2), stained with BODIPY 581/591 C11 (green, oxidized lipids; red, non-oxidized lipids) and Hoechst (nuclei in blue) and analysed by microscopy. Oxidation of the polyunsaturated butadienyl portion of BODIPY 581/591 C11 results in a shift of the fluorescence emission peak from ~590 nm (red) to ~510 nm (green). Scale bars, 20 μm. **b**, Quantification of lipid peroxidation expressed as the percentage of oxidized lipids from a; *n* biologically independent replicates per group (left to right) = 7, 8, 7, 8, 7, 7, 8 and 6. **c**, Representative confocal microscopy images showing oxidized and non-oxidized lipids in A549 cells previously transduced with either an empty vector control (Tet-pLKO-puro, shControl) or a doxycycline-inducible shRNA against *PLCG1* (shPLCγ1-2). Cells were then treated with doxycycline for 24 h and transfected with either pcDNA3.1 empty vector or pcDNA3.1-MCU-Flag. After this, cells were incubated for an additional 48 h in normoxia or hypoxia (1% O_2), stained with BODIPY 581/591 C11 (green, oxidized lipids; red, non-oxidized lipids) and Hoechst (nuclei in blue) and analysed by microscopy. Scale bars, 20 μm. **d**, Quantification of lipid peroxidation, expressed as the percentage of oxidized lipids from **c**; *n* biologically independent replicates per group (left to right) = 4, 7, 6, 11, 12, 11, 11 and 10. Graphical data are shown as the mean ± s.d. Statistical analyses were done using one-way ANOVA. $^{****}P < 0.0001$. Statistical source data are provided in the source data.

tumours from *Kras*$^{G12D/WT}$;*p53*$^{flox/flox}$;*Plcg1*$^{flox/flox}$ mice compared with *Kras*$^{G12D/WT}$;*p53*$^{flox/flox}$;*Plcg1*$^{wt/wt}$ mice (Fig. 7g). Moreover, tumour histological examination, IHC staining and immunoblotting against a LD marker, adipose differentiation-related protein (ADRP), revealed that *Plcg1* deletion led to a notable increase in tumour LD accumulation (Fig. 7h–j).

Overall, our results suggest that the suppression of PLCγ1 promotes KRAS-induced lung cancer.

Low PLCγ1 expression levels correlate with poor patient survival and high expression of hypoxia markers. Kaplan–Meier analysis of the human lung adenocarcinoma subset (LUAD) from The Cancer Genome Atlas (TCGA)[42] revealed that *PLCG1* expression positively correlated with patient overall survival (Fig. 8a). Notably, stratification of the LUAD cohort based on *KRAS* status into wild type and mutant KRAS showed that the shorter patient survival related to the *PLCG1*

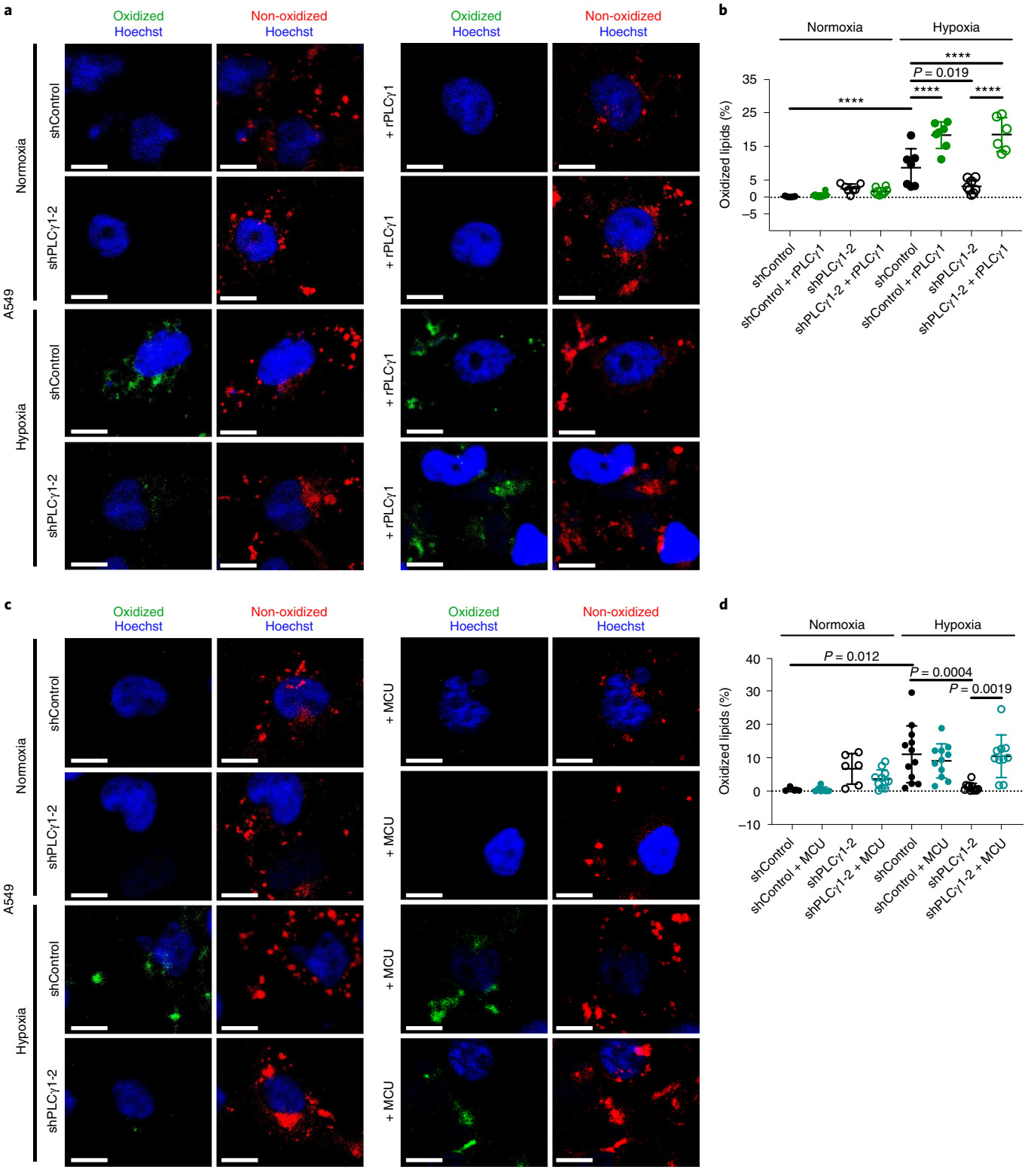

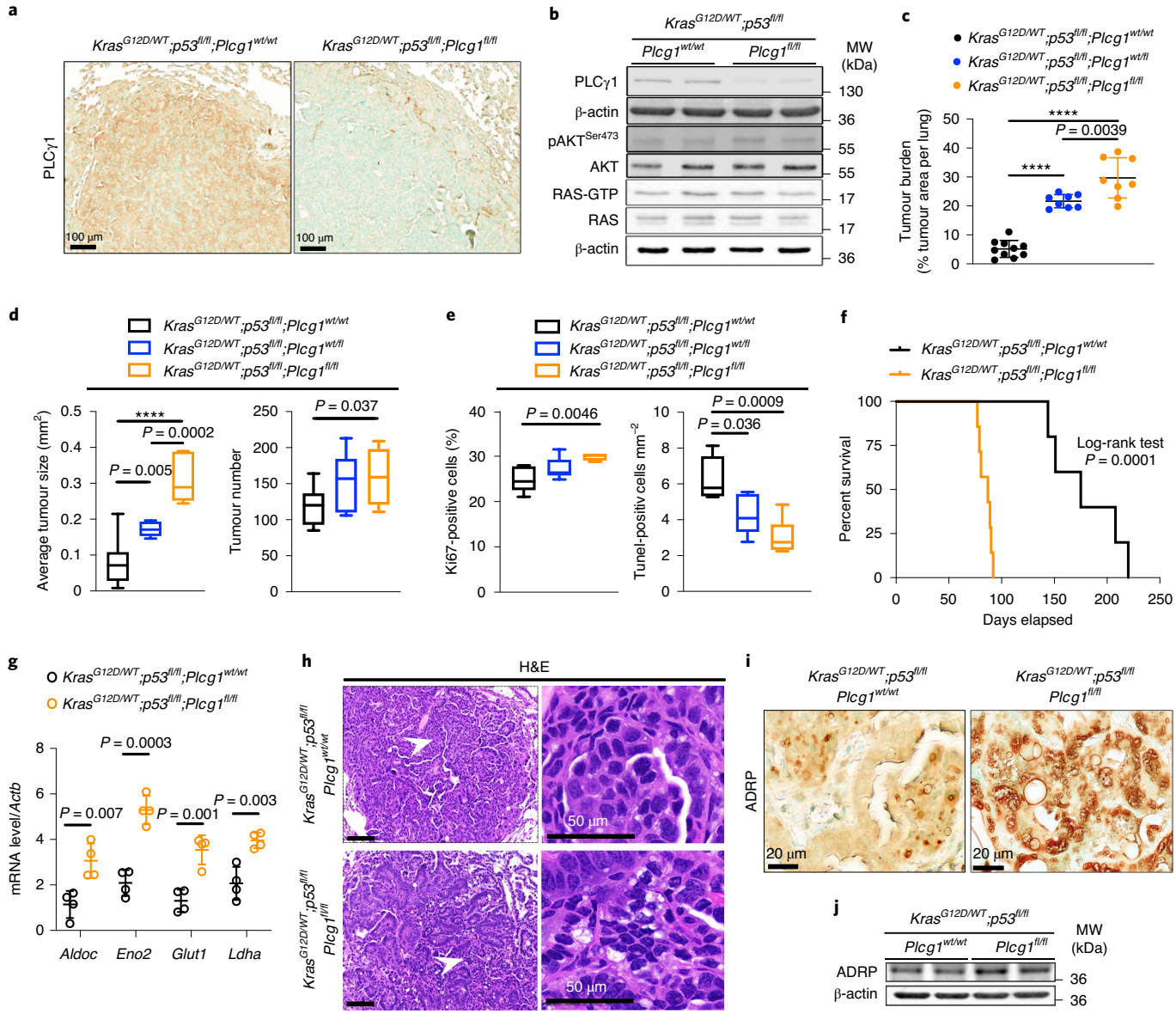

Fig. 7 | *Plcg1* deletion accelerates Kras-driven lung tumorigenesis and results in poor survival. a, Representative images of IHC against PLCγ1 in mouse lung tissue of the indicated mice 10 weeks after Cre induction. **b**, Representative immunoblot analysis of the indicated targets and RAS activity assay (bottom) in dissected lung tumours of the indicated mice treated as in **a**. **c**, Lung tumour burden quantification of mice with the indicated genotype 10 weeks after Cre induction; *n* mice per group (top to bottom): 10, 8 and 8. **d**, Average lung tumour size and tumour number of mice with the indicated genotype 10 weeks after Cre induction. Tumour size *n* mice per group (top to bottom): 10, 7 and 7; tumour number *n* mice per group (top to bottom): 10, 8 and 7. The boxplots span from the first to third quartile (depicting the median as a line in the middle), the whiskers extend to 1.5× the interquartile range (IQR). **e**, Quantification of Ki67 and number of Tunel-positive cells in mouse lung tumours from *LSL-Kras*$^{G12D/WT}$;*p53*$^{flox/flox}$;*Plcg1*$^{wt/wt}$ ($n=5$ mice), *LSL-Kras*$^{G12D/WT}$;*p53*$^{flox/flox}$;*Plcg1*$^{wt/flox}$ ($n=8$ mice for Ki67 and 5 mice for Tunel) and *LSL-Kras*$^{G12D/WT}$;*p53*$^{flox/flox}$;*Plcg1*$^{flox/flox}$ ($n=5$ mice for Ki67 and 6 mice for Tunel) mice, 10 weeks after Cre induction. The boxplots span from the first to third quartile (depicting the median as a line in the middle). **f**, Kaplan–Meier analysis showing the percent survival of *LSL-Kras*$^{G12D/WT}$;*p53*$^{flox/flox}$;*Plcg1*$^{wt/wt}$ ($n=7$ mice per group) and *LSL-Kras*$^{G12D/WT}$;*p53*$^{flox/flox}$;*Plcg1*$^{flox/flox}$ ($n=8$ mice per group) mice. Statistical analysis was done using log-rank (Mantel–Cox) test. **g**, mRNA level of the indicated genes from dissected mouse lung tumours of the indicated mice 10 weeks after Cre induction; $n=4$ mice per group. **h**, H&E staining of mice with the indicated genotype 10 weeks after Cre induction. The white arrowheads mark the magnified area on the right. Scale bars, 100 μm (left). **i**,**j**, Representative images of IHC (**i**) and immunoblot (**j**) for ADRP in mouse lung cancer tissue of the indicated genotype 10 weeks after Cre induction. Graphical data are shown as the mean ± s.d. Statistical analyses were done using two-tailed unpaired Student's *t*-test or one-way ANOVA. ****$P<0.0001$. Statistical source data and unprocessed immunoblots are provided in the source data.

expression level was associated with the cohort with mutations in *KRAS* (Fig. 8b).

Low *PLCG1* expression levels in lung tumours from the cohort with *KRAS* mutations was associated with high expression of several hypoxia markers implicated in glycolytic metabolism, such as *GLUT1*, aldolase A (*ALDOA*), phosphoglycerate kinase 1 (*PGK1*) and *LDHA* (Fig. 8c).

To assess PLCγ1 protein levels in human lung cancer, we performed IHC for PLCγ1 in a human lung adenocarcinoma tissue microarray and found that out of 199 samples, 124 samples were

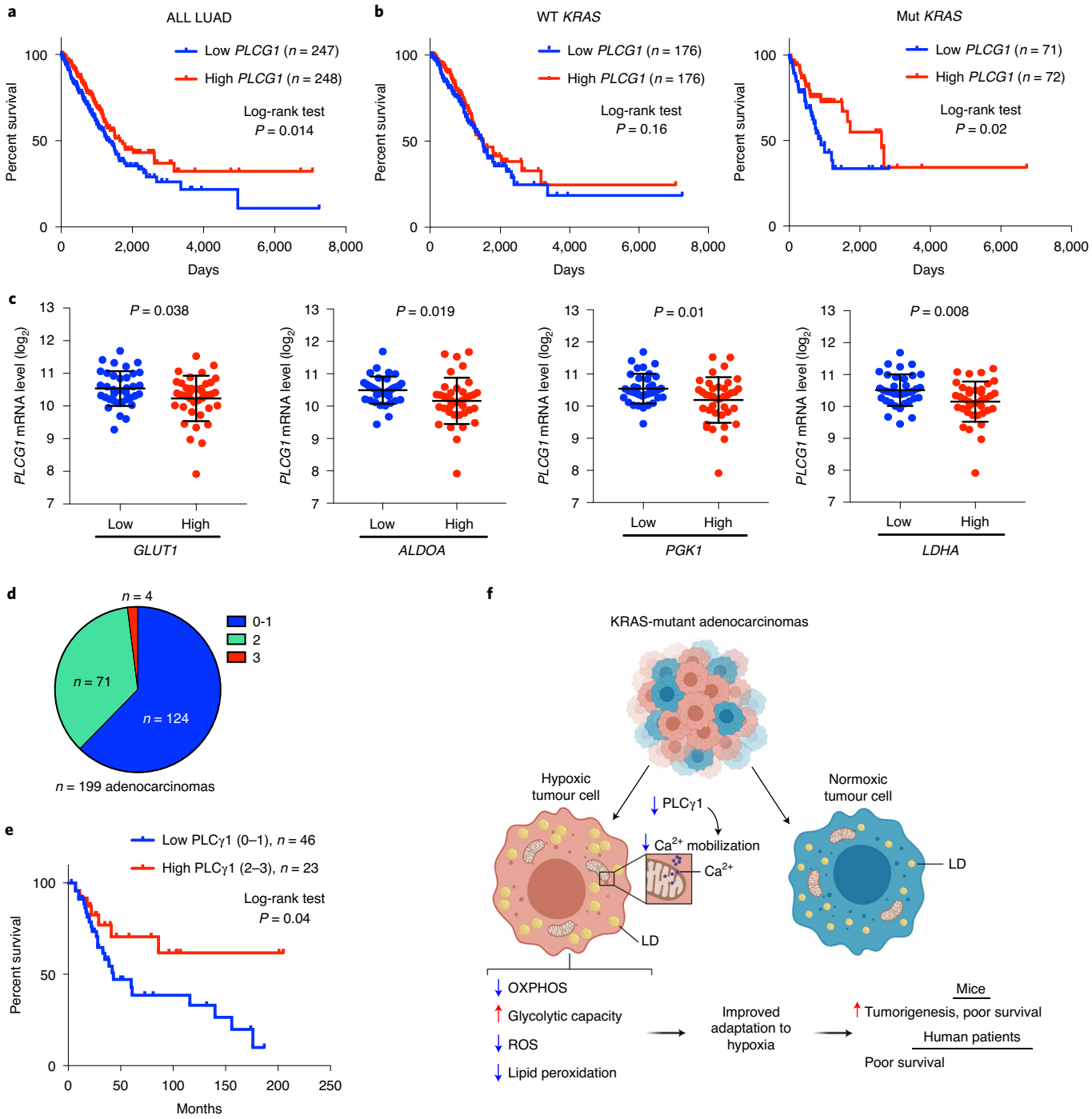

Fig. 8 | Low PLCγ1 levels in human lung adenocarcinomas correlate with poor patient survival. a,**b**, Kaplan–Meier analysis from TCGA (subset LUAD) database containing 495 human lung adenocarcinomas showing the percent survival of *PLCG1*-low versus *PLCG1*-high lung adenocarcinomas, subset LUAD (**a**, All LUAD) and after separation of the LUAD cohort into wild type *KRAS* (WT *KRAS*) or mutant *KRAS* (Mut *KRAS*) cohorts (**b**). The stratification in high/low expressing groups were performed by median separation. The number of patients and statistical significance are indicated. Statistical analyses were done using log-rank (Mantel–Cox) test. **c**, Expression of *PLCG1* ($\log_2$) after quartile-based separation of the mutant KRAS patient cohort from **b** into *GLUT1*, *ALDOA*, *PGK1* and *LDHA* low ($n=36$) versus high ($n=37$) expression corresponding to the first and the fourth quartile, respectively. The data are presented as the mean ± s.d. Statistical analyses were done using two-tailed unpaired Student's *t*-test. **d**, Pie chart showing the number of patients with high PLCγ1 protein levels (score 3; $n=4$), moderate (score 2; $n=71$) or negative to very low (score 0–1; $n=124$) from a TMA comprising 199 human lung adenocarcinomas. The TMA was processed for IHC against total PLCγ1 and the staining intensity was scored by a pathologist. Validation of the antibody is reported in Extended Data Fig. 10a. **e**, Kaplan–Meier analysis showing the percent survival of PLCγ1-low versus PLCγ1-high lung adenocarcinomas for the patients with known survival information that succumbed to lung cancer ($n=23$ PLCγ1-high and $n=46$ PLCγ1-low) from the TMA described in **d**. For the rest of the patients, either complete survival information was not available or they succumbed to other causes. The number of patients and statistical significance are indicated. Statistical analysis was done using log-rank (Mantel–Cox) test. **f**, Working model for the improved adaptation of cancer cells to hypoxia by PLCγ1 suppression. In hypoxia, PLCγ1 is suppressed, leading to decreased Ca^{2+} entry into the mitochondria, decreased OXPHOS, ROS and lipid peroxidation while increasing glycolysis. LD, lipid droplet. Illustration created with biorender.com. *n*, number of patients. Statistical source data are provided in the source data.

either negative or poorly stained for PLCγ1 (62%, score 0–1), 71 showed moderate staining intensity (35%, score 2) and only 4 samples (3%, score 3) showed high PLCγ1 protein levels (Fig. 8d and Extended Data Fig. 10a,b). These data strongly indicate that the majority of human lung adenocarcinomas have very low PLCγ1 protein levels, thus providing additional significance to our findings. Remarkably, Kaplan–Meier analysis of these patient samples stratified on the basis of low (score 0–1) and high (score 2–3) PLCγ1 protein levels showed that low PLCγ1 protein levels are associated with poor patient survival (Fig. 8e).

Taken together, these results suggest that the level of PLCγ1 has a predictive value for overall tumour resilience and patient survival.

Discussion

Hypoxia is a powerful driver of aggressive behaviour in solid cancers and is linked to metabolic reprogramming, with suppression of mitochondrial respiration in favour of glycolysis[43,44]. In KRAS-driven lung cancer, this metabolic adaptation to hypoxia has been extensively attributed to the effect of HIF1-dependent signalling and transcriptional regulation[8]. Here, we discovered that in mutant-KRAS-driven lung cancer, the suppression of mitochondrial respiration during hypoxia is highly dependent on PLCγ1 suppression; an effect linking changes of membrane phosphoinositide signalling with a decrease in mitochondrial Ca^{2+} and oxidative capacity (Fig. 8f).

Previous evidence revealed that in MEFs, PLCγ1 attenuates H_2O_2-induced ROS in normoxia[45]. These data are in line with our results in normoxia showing that PLCγ1 suppression triggers ROS, while its re-expression reduces ROS. These results uncover a role of PLCγ1 in which, in normoxia, it is required to prevent ROS by providing Ca^{2+} to maintain proper cellular and mitochondrial functionality, while in hypoxia, PLCγ1 must be suppressed to reduce mitochondrial Ca^{2+} and prevent damage.

A few reports suggest that PLCγ1 loss-of-function exerts antitumour actions in other solid cancer models such as breast, prostate, and head and neck squamous cell carcinomas[46–48]. Furthermore, high *PLCG1* expression levels are associated with poor patient survival in hepatocellular carcinoma[49]. Thus, future studies are warranted to understand whether the significance of our findings in cancer hypoxia and tumorigenesis is specific to KRAS-mutant lung cancer or is broader.

The suppression of PLCγ1 causes a significant accumulation of LDs, an effect that is expected to exert additional antioxidant effects by reducing substrates for FAO (hence hindering ROS formation) and by directly preventing lipid peroxidation[10,50–52]. Thus, it is tempting to speculate that the significance of PLCγ1 inhibition during hypoxia can be even greater in contexts during which ROS levels are strongly elevated in cancer cells, such as radiation treatment or chemotherapy[53]. Future investigation will be necessary to directly test whether PLCγ1 suppression underlies the resistance of hypoxic tumours to therapy.

Online content

Any methods, additional references, Nature Research reporting summaries, source data, extended data, supplementary information, acknowledgements, peer review information; details of author contributions and competing interests; and statements of data and code availability are available at https://doi.org/10.1038/s41556-020-00592-8.

Received: 27 June 2019; Accepted: 15 September 2020;
Published online: 19 October 2020

References

1. Thomlinson, R. H. & Gray, L. H. The histological structure of some human lung cancers and the possible implications for radiotherapy. *Br. J. Cancer* **9**, 539–549 (1955).
2. Brown, J. M. & Wilson, W. R. Exploiting tumour hypoxia in cancer treatment. *Nat. Rev. Cancer* **4**, 437–447 (2004).
3. Bhandari, V. et al. Molecular landmarks of tumor hypoxia across cancer types. *Nat. Genet.* **51**, 308–318 (2019).
4. Kamphorst, J. J. et al. Hypoxic and Ras-transformed cells support growth by scavenging unsaturated fatty acids from lysophospholipids. *Proc. Natl Acad. Sci. USA* **110**, 8882–8887 (2013).
5. Bensaad, K. et al. Fatty acid uptake and lipid storage induced by HIF-1α contribute to cell growth and survival after hypoxia–reoxygenation. *Cell Rep.* **9**, 349–365 (2014).
6. Botto, L. et al. Hypoxia-induced modifications in plasma membranes and lipid microdomains in A549 cells and primary human alveolar cells. *J. Cell. Biochem.* **105**, 503–513 (2008).
7. Huang et al. HIF-1-mediated suppression of acyl-CoA dehydrogenases and fatty acid oxidation is critical for cancer progression. *Cell Rep.* **8**, 1930–1942 (2014).
8. Semenza, G. L. HIF-1 mediates metabolic responses to intratumoral hypoxia and oncogenic mutations. *J. Clin. Invest.* **123**, 3664–3671 (2013).
9. Listenberger, L. L. et al. Triglyceride accumulation protects against fatty acid-induced lipotoxicity. *Proc. Natl Acad. Sci. USA* **100**, 3077–3082 (2003).
10. Bailey, A. P. et al. Antioxidant role for lipid droplets in a stem cell niche of *Drosophila*. *Cell* **163**, 340–353 (2015).
11. D'Souza, K. & Epand, R. M. Enrichment of phosphatidylinositols with specific acyl chains. *Biochim. Biophys. Acta* **1838**, 1501–1508 (2014).
12. Wymann, M. P. & Schneiter, R. Lipid signalling in disease. *Nat. Rev. Mol. Cell Biol.* **9**, 162–176 (2008).
13. Balla, T. Phosphoinositides: tiny lipids with giant impact on cell regulation. *Physiol. Rev.* **93**, 1019–1137 (2013).
14. Saliakoura, M. et al. The ACSL3–LPIAT1 signaling drives prostaglandin synthesis in non-small cell lung cancer. *Oncogene* **39**, 2948–2960 (2020).
15. Bunney, T. D. & Katan, M. Phosphoinositide signalling in cancer: beyond PI3K and PTEN. *Nat. Rev. Cancer* **10**, 342–352 (2010).
16. Schramp, M., Hedman, A., Li, W., Tan, X. & Anderson, R. PIP kinases from the cell membrane to the nucleus. *Subcell. Biochem.* **58**, 25–59 (2012).
17. Koss, H., Bunney, T. D., Behjati, S. & Katan, M. Dysfunction of phospholipase Cγ in immune disorders and cancer. *Trends Biochem. Sci.* **39**, 603–611 (2014).
18. Zhong, H. et al. Modulation of hypoxia-inducible factor 1alpha expression by the epidermal growth factor/phosphatidylinositol 3-kinase/PTEN/AKT/FRAP pathway in human prostate cancer cells: implications for tumor angiogenesis and therapeutics. *Cancer Res.* **60**, 1541–1545 (2000).
19. Mazure, N. M., Chen, E. Y., Laderoute, K. R. & Giaccia, A. J. Induction of vascular endothelial growth factor by hypoxia is modulated by a phosphatidylinositol 3-kinase/Akt signaling pathway in Ha-ras-transformed cells through a hypoxia inducible factor-1 transcriptional element. *Blood* **90**, 3322–3331 (1997).
20. Ferrer, I. et al. KRAS-mutant non-small cell lung cancer: from biology to therapy. *Lung Cancer* **124**, 53–64 (2018).
21. Salem, A. et al. Targeting hypoxia to improve non-small cell lung cancer outcome. *J. Natl Cancer Inst.* **110**, 14–30 (2018).
22. Gazdar, A. F., Girard, L., Lockwood, W. W., Lam, W. L. & Minna, J. D. Lung cancer cell lines as tools for biomedical discovery and research. *J. Natl Cancer Inst.* **102**, 1310–1321 (2010).
23. Uhlen, M. et al. Proteomics. Tissue-based map of the human proteome. *Science* **347**, 1260419 (2015).
24. Li, L. et al. Integrated omic analysis of lung cancer reveals metabolism proteome signatures with prognostic impact. *Nat. Commun.* **5**, 5469 (2014).
25. Marino, S., Vooijs, M., van Der Gulden, H., Jonkers, J. & Berns, A. Induction of medulloblastomas in p53-null mutant mice by somatic inactivation of Rb in the external granular layer cells of the cerebellum. *Genes Dev.* **14**, 994–1004 (2000).
26. Jackson, E. L. et al. Analysis of lung tumor initiation and progression using conditional expression of oncogenic K-ras. *Genes Dev.* **15**, 3243–3248 (2001).
27. Toker, A. & Cantley, L. C. Signalling through the lipid products of phosphoinositide-3-OH kinase. *Nature* **387**, 673–676 (1997).
28. Hicks, S. N. et al. General and versatile autoinhibition of PLC isozymes. *Mol. Cell* **31**, 383–394 (2008).
29. Bunney, T. D. et al. Structural and functional integration of the PLCγ interaction domains critical for regulatory mechanisms and signaling deregulation. *Structure* **20**, 2062–2075 (2012).
30. Rutter, G. A. et al. Subcellular imaging of intramitochondrial Ca^{2+} with recombinant targeted aequorin: significance for the regulation of pyruvate dehydrogenase activity. *Proc. Natl Acad. Sci. USA* **93**, 5489–5494 (1996).
31. Jouaville, L. S., Pinton, P., Bastianutto, C., Rutter, G. A. & Rizzuto, R. Regulation of mitochondrial ATP synthesis by calcium: evidence for a long-term metabolic priming. *Proc. Natl Acad. Sci. USA* **96**, 13807–13812 (1999).
32. Rimessi, A. et al. Interorganellar calcium signaling in the regulation of cell metabolism: a cancer perspective. *Semin. Cell. Dev. Biol.* **98**, 167–180 (2020).

33. Rana, R. S. & Hokin, L. E. Role of phosphoinositides in transmembrane signaling. *Physiol. Rev.* **70**, 115–164 (1990).
34. Rhee, S. G. & Bae, Y. S. Regulation of phosphoinositide-specific phospholipase C isozymes. *J. Biol. Chem.* **272**, 15045–15048 (1997).
35. Rimessi, A., Giorgi, C., Pinton, P. & Rizzuto, R. The versatility of mitochondrial calcium signals: from stimulation of cell metabolism to induction of cell death. *Biochim. Biophys. Acta* **1777**, 808–816 (2008).
36. Guzy, R. D. et al. Mitochondrial complex III is required for hypoxia-induced ROS production and cellular oxygen sensing. *Cell Metab.* **1**, 401–408 (2005).
37. Dada, L. A. et al. Hypoxia-induced endocytosis of Na,K-ATPase in alveolar epithelial cells is mediated by mitochondrial reactive oxygen species and PKC-ζ. *J. Clin. Invest.* **111**, 1057–1064 (2003).
38. Tarasov, A. I., Griffiths, E. J. & Rutter, G. A. Regulation of ATP production by mitochondrial Ca^{2+}. *Cell Calcium* **52**, 28–35 (2012).
39. Baughman, J. M. et al. Integrative genomics identifies MCU as an essential component of the mitochondrial calcium uniporter. *Nature* **476**, 341–345 (2011).
40. Giorgi, C., Marchi, S. & Pinton, P. The machineries, regulation and cellular functions of mitochondrial calcium. *Nat. Rev. Mol. Cell Biol.* **19**, 713–730 (2018).
41. Negre-Salvayre, A., Coatrieux, C., Ingueneau, C. & Salvayre, R. Advanced lipid peroxidation end products in oxidative damage to proteins. Potential role in diseases and therapeutic prospects for the inhibitors. *Br. J. Pharmacol.* **153**, 6–20 (2008).
42. Cancer Genome Atlas Research Network. Comprehensive molecular profiling of lung adenocarcinoma. *Nature* **511**, 543–550 (2014).
43. Wilson, W. R. & Hay, M. P. Targeting hypoxia in cancer therapy. *Nat. Rev. Cancer* **11**, 393–410 (2011).
44. Dewhirst, M. W., Cao, Y. & Moeller, B. Cycling hypoxia and free radicals regulate angiogenesis and radiotherapy response. *Nat. Rev. Cancer* **8**, 425–437 (2008).
45. Wang, X. T., McCullough, K. D., Wang, X. J., Carpenter, G. & Holbrook, N. J. Oxidative stress-induced phospholipase C-γ1 activation enhances cell survival. *J. Biol. Chem.* **276**, 28364–28371 (2001).
46. Sala, G. et al. Phospholipase Cγ1 is required for metastasis development and progression. *Cancer Res.* **68**, 10187–10196 (2008).
47. Thomas, S. M. et al. Epidermal growth factor receptor-stimulated activation of phospholipase Cγ-1 promotes invasion of head and neck squamous cell carcinoma. *Cancer Res.* **63**, 5629–5635 (2003).
48. Turner, T., Epps-Fung, M. V., Kassis, J. & Wells, A. Molecular inhibition of phospholipase cγ signaling abrogates DU-145 prostate tumor cell invasion. *Clin. Cancer Res.* **3**, 2275–2282 (1997).
49. Tang, W. et al. Oncogenic role of phospholipase C-γ1 in progression of hepatocellular carcinoma. *Hepatol. Res.* **49**, 559–569 (2019).
50. Ackerman, D. et al. Triglycerides promote lipid homeostasis during hypoxic stress by balancing fatty acid saturation. *Cell Rep.* **24**, 2596–2605.e5 (2018).
51. Zhang, X. et al. Inhibition of intracellular lipolysis promotes human cancer cell adaptation to hypoxia. *eLife* **6**, e31132 (2017).
52. Liu, L. et al. Glial lipid droplets and ROS induced by mitochondrial defects promote neurodegeneration. *Cell* **160**, 177–190 (2015).
53. Teppo, H. R., Soini, Y. & Karihtala, P. Reactive oxygen species-mediated mechanisms of action of targeted cancer therapy. *Oxid. Med. Cell. Longev.* **2017**, 1485283 (2017).

Methods

Reagents and plasmids. When indicated, knockdown of the protein of interest was induced by administration of 1 μg ml^{-1} doxycycline (Fisher Scientific, BP2653) in the culture medium. The rat pcDNA3.1-HA-LIC-PLCγ1 plasmid was a gift from J. Sondek[54] (UNC Center for Structural Biology, Chapel Hill, USA) and was used to transfect the MEFs. The human pcDNA3.1-PLCγ1 and the shRNA-rPLCγ1 constructs that were used to trasfect human cells were custom-made by Genscript. The pcDNA3.1-MCU-Flag was provided by P. Pinton[55]. For the xenograft experiment in Fig. 5g, we moved the MCU–Flag from the pcDNA3.1-MCU–Flag into pWZL-Hygro using BamHI/EcoRI restriction sites to generate pWZL-Hygro-MCU–Flag. The tet-pLKO-puro was a gift from D. Wiederschain (Addgene, plasmid 21915)[56]. pLKO.1 puro (Addgene, plasmid 8453), pCMV-VSV-G (Addgene, plasmid 8454) and pCMV-dR8.2 dvpr (Addgene, plasmid 8455) were gifts from B. Weinberg[57]. pMSCVhygro-Cre was a gift from K. Ge (Addgene, plasmid 34565)[58]. The shRNAs were obtained from Sigma Aldrich and cloned into the Tet-pLKO-puro backbone plasmid after digestion with AgeI/EcoRI. All the constructs were confirmed by sequencing.

Cell lines. The human lung adenocarcinoma cell lines used in this study (A549, H358 and A427) were derived from male patients and were gifts from J. Minna (UT Southwestern Medical Center)[59]. HEK293T cells were obtained from the American Type Culture Collection (CRL-11268). All cell lines were DNA fingerprinted for provenance and tested negative for mycoplasma. Cells were cultured in an incubator at 37 °C and 5% CO_2 in RPMI-1640 medium or DMEM (for HEK293T) containing 10% fetal bovine serum (Thermo Fisher), 100 IU ml^{-1} penicillin and 100 μg ml^{-1} streptomycin (Gibco). MEFs were generated by crossing a *Kras*$^{G12D/WT}$;*p53*$^{flox/flox}$;*Plcg1*$^{wt/flox}$ male mouse with a *Kras*$^{G12D/WT}$;*p53*$^{flox/flox}$;*Plcg1*$^{wt/flox}$ female mouse. Concomitant *Kras*$^{G12D/WT}$ induction, *p53* and, where applicable, *Plcg1* deletion was achieved by infection with pMSCV-hygro-Cre virus followed by selection with 150 μg ml^{-1} hygromycin.

Animal studies. Mice were maintained under a temperature of 21 ± 2 °C and humidity of 50 ± 10% with a standard 12-h light–dark cycle and were fed ad libitum. Genotyping was performed using a KAPA HotStart Mouse Genotyping kit (Kapa Biosystems, KK7352) and a KAPA2G Fast HotStart Genotyping mix (Kapa Biosystems, KK5621) according to the manufacturer's instructions. The mouse genotypes were confirmed following the corresponding Jackson Laboratory protocols. PCR assays for the *Plcg1* genotyping were performed with an annealing temperature of 60 °C. A complete list of oligonucleotides used to genotype the mice is provided in Supplementary Table 1.

For intratracheal administration, 2.5×10^7 infectious particles of VVC-U of Iowa-5 Ad5CMVCre (Viral Vector Core, University of Iowa) were delivered to male mice at 8 weeks of age. Mice were killed 10 weeks post induction and lungs were retrieved after anaesthesia and perfusion. Tissue for histology was fixed overnight in 4% paraformaldehyde at 4 °C before paraffin embedding. Tissue for western blotting and mRNA analysis was snap frozen in liquid nitrogen.

For the xenotransplantation studies in vivo, 1×10^6 MEF cells (*Kras*$^{G12D/WT}$;*p53*$^{flox/flox}$;*Plcg1*$^{wt/wt}$, *Kras*$^{G12D/WT}$;*p53*$^{flox/flox}$;*Plcg1*$^{wt/flox}$ or *Kras*$^{G12D/WT}$;*p53*$^{flox/flox}$;*Plcg1*$^{flox/flox}$) or A549 cells were subcutaneously injected into male *NOD.Cg-Prkdc*^{scid} *Il2rg*^{tm1Wjl}/*SzJ* (NSG, stock number 005557)[60,61] mice at 6–8 weeks of age. Doxycycline was provided in the water of the mice. The mice were closely monitored on a daily basis, and the size of the tumours was measured with a caliper every 2–3 days. Mice were killed when the tumour volume reached 1,000 mm^3. To investigate tumour tissue hypoxia, mice were intraperitoneally injected with a Hypoxyprobe-1 (pimonidazole HCl) solution (Hypoxyprobe Green kit, HP6-200) at a dosage of 60 mg per kg body weight, 30 min before euthanasia. A complete list of antibodies used is provided in Supplementary Table 1.

Mixed background *LSL-Kras*$^{G12D/WT}$;*p53*$^{flox/flox}$ mice were generated by crossing stock *B6.129SS4-kras*^{tm4Tyj}/*J* (from The Jackson Laboratory, stock number 008179)[26] mice with *B6.129P2-Trp53*^{tm1Brn}/*J* (from The Jackson Laboratory, stock number 008462) mice[25]. The mixed background Cre-inducible *LSL-Kras*$^{G12D/WT}$;*p53*$^{flox/flox}$;*Plcg1*$^{flox/flox}$ mouse model was obtained by crossing *LSL-Kras*$^{G12D/WT}$;*p53*$^{flox/flox}$ mice with *B6(Cg)-Plcg1tm1Flh/J* (*Plcγ1* $^{flox/flox}$) mice. The *Plcg1*$^{flox/flox}$ mice were provided by T.M.S. and F.H.H. The *LSL-Kras*$^{G12D/WT}$;*p53*$^{flox/flox}$;*Plcg1*$^{flox/wt}$ mice were backcrossed for eight generations before creating the experimental groups. Only male littermates were used for the experiments. The study was compliant with all relevant ethical regulations regarding animal research. Experimental procedures were approved by the cantonal veterinary commission and animal welfare officer from the Veterinaerdienst des Kantons Bern.

shRNAs, virus production and transduction. Recombinant lentiviruses were produced by transfecting HEK293T cells with pCMV-VSV-G (VSV-G protein), pCMV-dR8.2 (lentivirus packaging vector) and lentiviral constructs using *Trans*IT-293 transfection reagent (Mirus, MIR2705) according to the manufacturer's instructions. Retroviruses were produced by transfecting Ampho cells, using *Trans*IT®-293 transfection reagent, according to the manufacturer's instructions. A complete list of shRNA sequences is provided in Supplementary Table 1.

Reverse transcription and qPCR. RNA was extracted using a RNAeasy kit (Qiagen, 74104) and complementary DNA was synthesized with a RevertAid First Strand cDNA synthesis kit (Thermo Scientific, K1622). qPCR was performed in 96-well plates (TreffLab) with FastSybr green (Thermo Scientific, 4367659). Normalization was performed using the ΔΔCT method. A full list of the oligonucleotides used is provided in Supplementary Table 1.

IHC analysis. IHC was conducted on paraffin-embedded tissue. All sections used for histological analysis were 5-μm thick. Histological characterization and consequent scoring of neoplastic lesion grades of haematoxylin and eosin (H&E)-stained sections of lungs were done with supervision and confirmed by a pathologist. Tumour burden was assessed via digital quantification of the area occupied by tumours compared to unaffected tissue using QuPath (open-source software, v.0.1.2). Sections were deparaffinized, rehydrated through a graded series of alcohol and subjected to antigen retrieval by boiling for 10 min in antigen-retrieval sodium citrate buffer (pH 6). Sections were then pretreated for 30 min with 3% H_2O_2 (Sigma-Aldrich, 216763) in PBS, washed twice with 0.1 M Tris-buffered saline (TBS), blocked for 1 h in 2% BSA in TBS containing 0.1% Polysorbate 20 (TBS-T), 10 min in 2.5% normal horse serum (Vector, S-2012) and incubated with primary antibodies diluted appropriately in blocking solution. The following day, sections were washed in TBS-T, incubated with ready to use secondary antibody (Vector, MP-7401) for 1 h or with Mouse on Mouse ImmPRESS Peroxidase Polymer Anti-Mouse reagent (Vector, MPX-2402) for 10 min. The staining was revealed with DAB+ solution (Dako, K3467). Tissue sections were then counterstained with methyl green (Vector Labs, H-3402), dehydrated and mounted. Apoptotic cells were stained using the DeadEnd Colorimetric TUNEL system (Promega, G7360) according to the manufacturer's instructions. Stained sections were scanned using a Pannoramic Midi II digital slide scanner (3DHISTECH), and image analysis was performed using QuPath. A complete list of antibodies used for IHC is provided in Supplementary Table 1.

Human tumour tissue microarray staining and patient survival study. The patient-derived tumour tissue microarray (TMA) and patient survival information were provided by the Institute of Pathology, University of Bern and the University Hospital Basel. In the patient-derived TMA study, only patients diagnosed with lung adenocarcinomas and only after the first surgical resection without prior treatment were included. The patients were of mixed age and sex, and no selection was applied or any genotypic assessment (that is, *KRAS* mutation status) was performed. The use of human samples was approved by the Swiss Association of Research Ethics Committees (Swissethics), Institute: Kantonal Ethikkommission for research. The study was compliant with all relevant ethical regulations regarding research involving human participants and all samples were provided after patient consent. A full list of patient age and gender information is reported in Supplementary Table 2.

TMA IHC staining was carried out using the automated system BOND RX (Leica Biosystems). All sections were deparaffinized and rehydrated using Dewax solution (Leica Biosystems) at 72 °C for 30 s. Endogenous peroxidase activity was blocked with 3% H_2O_2 solution (Leica Biosystems) for 5 min. Samples were incubated with an anti-PLCγ1 primary antibody (Santa Cruz Biotechnology, sc-7290, clone) at room temperature for 30 min at 1:200 dilution. Antigen retrieval was performed using Tris-EDTA buffer (pH 9) and citrate buffer (pH 6) at 95 °C for 30 min. The slides were incubated with the secondary antibody using a Bond Polymer Refine kit (Leica Biosystems) for 15 min, incubated with the chromogen DAB (3-3′-diaminobenzidine) for 10 min, counterstained with haematoxylin for 5 min, and finally mounted with Aquatex (Merck Millipore). The TMA was scored by a pathologist specialized in lung pathology (S.A.B.). The intensity of PLCγ1 staining was highly homogeneous, and stains were scored semiquantitatively as scores 0–3 according to intensity. Scores 0–1 were considered negative to low and scores 2–3 were combined as high-expression pattern.

Immunofluorescence. For immunofluorescence, cells were washed and fixed in 4% paraformaldehyde for 15 min at room temperature. Cells were washed with PBS, permeabilized with PBS plus 0.1% TritonX-100 for 5 min and blocked with 5% BSA in PBS for 1 h at room temperature. Cells were then incubated with primary antibody diluted in 5% BSA in PBS for 2–3 h at room temperature. Primary antibody was detected with Alexa Fluor secondary antibody diluted 1:500 in PBS at room temperature for 1 h in the dark. For immunofluorescence conducted on paraffin-embedded tissue, all stainings with primary antibodies were done after deparaffinization, rehydration through a graded series of alcohol, antigen retrieval by boiling for 10 min in sodium citrate buffer (pH 6) and blocking in 2% BSA in PBS-T buffer. Antibodies were diluted in blocking solution and incubation was performed at 4 °C overnight. Secondary fluorescent-tagged antibodies were from Molecular Probes (Invitrogen). Stained cells and sections were scanned using a Pannoramic Midi II digital slide scanner (3DHISTECH).

RAS activity assay. For the detection of active RAS, 500 μg of mouse protein lysate was used, and the assay was performed using an Active Ras Detection kit according to the manufacturer's instructions (Cell Signaling Technology, 8821).

Immunoblotting. Cells were lysed in RIPA buffer (50 mM Tris-HCl pH 8.0, 150 mM NaCl, 1.0% NP-40, 0.5% sodium deoxycholate and 0.1% SDS) or NP40 buffer to detect phosphorylated proteins (50 mM Tris-HCl pH 8.0, 150 mM NaCl, 1% NP-40) containing complete EDTA-free protease inhibitors (Roche) and 1 mM phenylmethyl sulfonyl fluoride. Samples were resolved by SDS–PAGE in a Bio-Rad blotting chamber, transferred to nitrocellulose membranes using a semi-dry chamber (Bio-Rad) and blocked in 5% BSA. Membranes were then incubated overnight at 4 °C with primary antibody diluted in 5% BSA in TBS containing 0.1 % Tween. Secondary fluorescent-tagged antibodies were from Li-Cor Biosciences, and development was done in a Li-Cor fluorescence–chemiluminescence detector. All antibodies and their dilutions are listed in Supplementary Table 1.

Cell proliferation assay. Cell proliferation was measured as previously described[62]. Briefly, cells were plated at low confluency in 24-well plates (8,000 cells per well for A549 and MEFs and 9,000 cells per well for H358 and A427) and left to proliferate for 2, 4 or 6 days. For the hypoxia experiments, cells were placed in a hypoxia chamber (Whitley H35 HEPA Hypoxystation). Cell viability was measured by crystal violet (Sigma Aldrich) staining (0.1% in 20% methanol) of adherent cells after 10 min fixation in 4% paraformaldehyde (Sigma Aldrich). After washing twice and air-drying, stained cells were de-coloured with 10% acetic acid and OD600 values were measured with a spectrophotometer.

Caspase-3 activity assay. Caspase-3 activity was determined using an EnzChek Caspase-3 Assay kit #2 (Invitrogen, E13184). Knockdown was induced with doxycycline for 48 h. Following this period, the cells were cultured for 4 days in normoxic or hypoxic conditions as necessary. For every condition, the samples were run in triplicate using 1×10^6 cells per replicate. The assay was then performed according to the manufacturer's instructions and the results were normalized to the protein content.

ROS, LD and Ann/PI measurement by flow cytometry. For every flow cytometry analysis, cells were gated according to their forward and side scatter values to exclude cell clusters (see Supplementary Fig. 1 for gating information). For the experiments in which PLCγ1 was overexpressed, cells were transfected concomitantly with the start of knockdown induction. Following this period, 4.5×10^5 cells were plated and cultured for 24 h in normoxia or hypoxia (1% O_2, Whitley H35 HEPA Hypoxystation) as described in the related figure legends. To measure ROS levels, 1×10^6 cells were resuspended in 1 µM dihydrorhodamine 123 (DHR) (Sigma-Aldrich, D1054) in PBS and incubated for 30 min at 37 °C. To quench ROS, cells were treated with 10 µM MitoTEMPO for 18 h before staining. For LD measurement, 1×10^6 cells were gently washed with PBS and fixed with 4% paraformaldehyde for 10 min at room temperature. After removing the fixative solution, cells were washed two times with PBS to remove residual paraformaldehyde and stained with 1× LipidTOX Deep Red Neutral Lipid Stain solution (Invitrogen, H34477) for 30 min. The cells were then washed with PBS before performing the assay as previously described[63]. For the Ann/PI cell death assay, cells were plated at low confluency in a 12-well plate and treated as described in the figure legends. On the day of the assay, cells were washed with staining buffer (150 mM NaCl, 4 mM KCl, 2.5 mM $CaCl_2$, 1 mM $MgSO_4$, 15 mM HEPES pH 7.2, 2% FBS and 10 mM NaN_3) and stained with Atto633-conjugated Annexin V for 20 min in the dark, on ice. Cells were then washed with staining buffer and resuspended in 200 µl PI at a final concentration of 2 µg ml^{-1} (MEFs) or 40 µg ml^{-1} (A549). To inhibit caspase-induced cell death, cells were treated with 20 µM Q-VD-OPH 18 h before staining. Flow cytometry was performed following a standard procedure with a FACS Lyric instrument (BD Biosciences). Data were analysed using the FlowJo V10 workspace.

Ca^{2+} measurements. Endoplasmic Reticulum aequorin (erAEQ), mitochondrial aequorin (mtAEQ) and cytosolic aequorin (cytAEQ) are the Ca^{2+}-sensitive chimeric probes used to target the ER, the mitochondria and the cytosol, respectively[64]. To reconstitute the erAEQmut with high efficiency, the luminal $[Ca^{2+}]$ of the ER first had to be reduced. This was achieved by incubating the cells for 1 h at 4 °C in Krebs ringer buffer (KRB) supplemented with 5 µM coelenterazine, the Ca^{2+} ionophore ionomycin and 600 µM EGTA. After this incubation, cells were extensively washed with KRB supplemented with 2% BSA. For the experiments with cytAEQ and mtAEQ, cells were incubated with 5 µM coelenterazine for 1–2 h in modified KRB supplemented with 1 mM $CaCl_2$. All aequorin measurements were carried out in KRB supplemented with either 1 mM $CaCl_2$ (cytAEQ and mtAEQ) or 100 µM EGTA (erAEQmut). Then, the coverslip with transfected cells was placed in a perfused, thermostatic chamber located in close proximity of a low-noise photomultiplier, with a built-in amplifier discriminator. Histamine (100 µM) was added to the medium as an IP_3-dependent agonist to induce ER Ca^{2+} release and consequent intracellular Ca^{2+} mobilization. The experiments were terminated by lysing the cells with 100 µM digitonin in a hypotonic Ca^{2+}-containing solution (10 mM $CaCl_2$ in H_2O), thus discharging the remaining aequorin pool. The output of the discriminator was captured by a Thorn-EMI photon counting board for analyses. The aequorin luminescence data were calibrated offline into $[Ca^{2+}]$ values using a computer algorithm based on the Ca^{2+} response curve of wild-type and mutant aequorins[64]. The rate of ER Ca^{2+} release was calculated as second derivative of released $[Ca^{2+}]_{er}$ from the ER during agonist stimulation.

LD imaging. For imaging LDs and lipid peroxidation, 2×10^4 cells were plated on coverslips in 24-well plates.

For LD staining, cells were washed twice with PBS and fixed with 4% paraformaldehyde for 10 min at room temperature. After removing the fixative solution, cells were rinsed gently two to three times with PBS to remove residual paraformaldehyde and stained with 1× HCS LipidTOX Deep Red Neutral Lipid Stain solution (Invitrogen, H34477) for at least 30 min before imaging. For lipid peroxidation detection, live cells were incubated with 500 nM BODIPY 581/591 C11 (Invitrogen, D3861) for 30 min at 37 °C. The cells were then washed three times with PBS before imaging.

FAO assay. β-oxidation of fatty acids was measured as previously described[65]. Briefly, we plated 30×10^4 cells in 6-well plates and 18 h later, we incubated the cells with medium supplemented with [9,10-^{3}H]-palmitate (Hartmann Analytic, 1 mCi ml^{-1}) bound to 10% fatty-acid-free BSA (Sigma). A total of 3.3 µl of [9,10-^{3}H]-palmitate and 6.7 µl of fatty-acid-free BSA were used per 1 ml of cell culture medium and cultured for 24 h. After 24 h, supernatant was applied to ion-exchange columns (Dowex 1X8–200, Sigma), and tritiated water was recovered by eluting with 0.5 ml of H_2O. A 100-µl aliquot was then mixed with 100 µl of liquid scintillation cocktail and the amount of radioactivity released was measured using a Top count NXT liquid scintillation counter (Packard) in 96-well polystyrene plates (Nunc F96 microwell, Thermo). β-oxidation was expressed as counts per minute (c.p.m.) per milligram of protein.

Ultra-performance liquid chromatography–tandem mass spectrometry. *Sample processing.* Cells (2×10^6) were washed twice with PBS and incubated with 0.5 M trichloroacetic acid (TCA) for 5 min on ice. Cells were then scraped from the dish, vortexed for 30 s and further incubated on ice for 5 min. The TCA-treated samples were centrifuged at 20,000×*g* for 3 min at 4 °C. After discarding the supernatant, the pellet was resuspended in 1 ml of 5% (w/v) TCA + 10 mM EDTA and centrifuged at 20,000×*g* for 3 min at 4 °C. After repeating the same step once, the pellet was used for lipid extraction.

Lipid extraction. Before lipid extraction, the following lipid analytical internal standards were added to the TCA precipitates: 17:0-20:4 PI(4,5)P_2, 17:0-20:4 PI(3,4,5)P_3 and 17:0-20:4 PIP. Lipids were extracted using a modified acidified chloroform–methanol extraction protocol. It was initiated by adding 670 µl of chloroform:methanol:12 N HCl (40:80:1) to the TCA precipitate followed by vigorous vortexing for 5 min and incubation for 10 min at 4 °C. Then, 650 µl of ice-cold chloroform was added and the samples were vortexed for another 2 min and allowed to sit for 5 min at 4 °C, after which 300 µl of ice-cold 1 M HCl was added. The samples were vortexed for 2 min, centrifuged at 10,000×*g* for 2 min, and the lower phase was then collected in a fresh 2-ml microcentrifuge tube. Ice-cold theoretical lower phase (900 µl) was generated by combining a chloroform:methanol:1.74 M HCl mixture (86:14:1 v/v/v) and was added to the upper phase, and the mixture was vortexed and centrifuged. The lower phase was then combined with the previously collected lower phase and dried under a stream of N_2 and subsequently methylated as previously described[66].

Mass spectroscopy. Liquid chromatography–mass spectroscopy was carried out essentially as previously described[66].

Mass spectroscopy analysis and normalization. Peak areas for acyl-chain specific lipid species and standards were quantified by integrating mass spectroscopy curves as previously described[66]. The peak areas were normalized to the peak area of the corresponding synthetic lipid standard. Experimenters were blinded to the experimental conditions during data analysis.

OCR and ECAR measurements. Extracellular flux analysis of tumour cells in hypoxia was performed using an Agilent Seahorse XF^{e}96 Analyzer placed inside the hypoxia chamber (Whitley H35 HEPA Hypoxystation) stabilized at 3% O_2. Agilent recommends performing hypoxic assays in a ≥3 % ambient O_2 environment to prevent potential O_2 exhaustion and development of anoxic conditions within the microchamber during the assay. In all experiments, cells were incubated in normoxia or hypoxia (3% O_2) for 24 h, split, and 4.2×10^4 A549 cells or 1×10^4 MEF cells were seeded on Seahorse 96-well plates and incubated for an additional 24 h in normoxia or hypoxia before the Seahorse experiment. The OCR was determined during sequential treatments with oligomycin (2 µM, Sigma Aldrich, O4876), FCCP (1.5 µM, Abcam, ab120081) and rotenone/antimycin (1 µM, Sigma Aldrich, R8875, A8674), while the ECAR was determined during sequential treatments with glucose (10 mM), oligomycin and 2-deoxy-glucose (2DG, 100 mM, Sigma Aldrich, D3179) at the indicated time as shown in the related figure legends. To calculate the glycolysis and respiration parameters for each sample, the last OCR and ECAR readings obtained for each well after the injection of glucose, oligomycin or rotenone/antimycin were used. However, to correctly reflect the phenotype of the mutant cell lines, the average of several

determinations of the FCCP-induced OCRs and ECARs of each well was used as a basis for calculating the stressed glycolysis and OXPHOS activity. The final readings were normalized to the cell number.

TCGA data analysis. TCGA LUAD dataset was retrieved from the Genomic Data Commons Portal. The data were downloaded with the help of the web graphic user interface Xena browser https://xenabrowser.net and analysed using GraphPad Prism v.7.0. Incomplete data, missing expression values and/or survival were eliminated from the analysis, and only primary tumours were considered.

Quantifications and statistical analysis. *Statistics and reproducibility.* All datasets were organized and analysed in Microsoft Excel 2016 and GraphPad Prism v.7.0.0 (GraphPad Software, www.graphpad.com). All data presented are expressed as the mean ± s.d. (unless indicated in the figure legends) of three or more biologically independent replicates/group (the specific number is indicated in the related figure legends). All graphical in vitro data report one representative experiment from experiments performed independently at least three times (except for the mass-spectrometry-based lipidomics experiment, which was performed twice), with similar results obtained. The significance of the results was determined employing two-tailed unpaired Student's *t*-test (when comparing two groups) or one-way analysis of variance (ANOVA) with Tukey's correction for multiple comparisons (when more than two groups were compared) and significance is indicated in the related figure legends. For the cell proliferation data, only the figure-relevant statistical differences are represented. No outliers were found in any dataset and no animals or data were excluded from statistical analyses.

Colocalization analysis. The analyses were performed using the Imaris Studio Software (www.bitplane.com). To exclude false positivity due to the background of the green channel, a first mask was set on it with a threshold value of 1 for bright intensity. The analyses were run with the Imaris CoLoc tool and the results are the average of at least 15 pictures per condition. For the oxidized lipid analysis, the colocalization of the green channel (oxidized lipids) and the red channel (non-oxidized lipids) was assessed with automatic thresholding (CoLoc → auto thresholds). For the colocalization of pPLCγ1^{Tyr783} or PLCγ1 and pimonidazole, sections were scanned in automatic mode with a slide scanner and were used to score for the hypoxic versus nonhypoxic tumour areas without modifying the laser power and gain of the detector.

Reporting Summary. Further information on research design is available in the Nature Research Reporting Summary linked to this article.

Data availability

All supporting data are included in this published article and its Supplementary Information. Requests to use the PLCγ1 floxed mice will be redirected to F.H.H. and T.M.S. The Cancer Genome Atlas (TCGA) lung adenocarcinoma (LUAD) dataset was retrieved from the Genomic Data Commons Portal: http://cancergenome.nih.gov. The data were downloaded with the help of the web graphic user interface Xena browser https://xenabrowser.net. Source data are provided with this paper.

References

54. Gresset, A., Hicks, S. N., Harden, T. K. & Sondek, J. Mechanism of phosphorylation-induced activation of phospholipase C-γ isozymes. *J. Biol. Chem.* **285**, 35836–35847 (2010).
55. De Stefani, D., Raffaello, A., Teardo, E., Szabo, I. & Rizzuto, R. A forty-kilodalton protein of the inner membrane is the mitochondrial calcium uniporter. *Nature* **476**, 336–340 (2011).
56. Wiederschain, D. et al. Single-vector inducible lentiviral RNAi system for oncology target validation. *Cell Cycle* **8**, 498–504 (2009).
57. Stewart, S. A. et al. Lentivirus-delivered stable gene silencing by RNAi in primary cells. *RNA* **9**, 493–501 (2003).
58. Wang, L., Jin, Q., Lee, J. E., Su, I. H. & Ge, K. Histone H3K27 methyltransferase Ezh2 represses *Wnt* genes to facilitate adipogenesis. *Proc. Natl Acad. Sci. USA* **107**, 7317–7322 (2010).
59. Phelps, R. M. et al. NCI-Navy medical oncology branch cell line data base. *J. Cell Biochem. Suppl.* **24**, 32–91 (1996).
60. Coughlan, A. M. et al. Myeloid engraftment in humanized mice: impact of granulocyte-colony stimulating factor treatment and transgenic mouse strain. *Stem Cells Dev.* **25**, 530–541 (2016).
61. Shultz, L. D. et al. Human lymphoid and myeloid cell development in NOD/LtSz-*scid IL2Rγ*^{null} mice engrafted with mobilized human hemopoietic stem cells. *J. Immunol.* **174**, 6477–6489 (2005).
62. Ramadori, G. et al. Diet-induced unresolved ER stress hinders KRAS-driven lung tumorigenesis. *Cell Metab.* **21**, 117–125 (2015).
63. Majka, S. M. et al. Analysis and isolation of adipocytes by flow cytometry. *Methods Enzymol.* **537**, 281–296 (2014).
64. Bonora, M. et al. Subcellular calcium measurements in mammalian cells using jellyfish photoprotein aequorin-based probes. *Nat. Protoc.* **8**, 2105–2118 (2013).
65. Padanad, M. S. et al. Fatty acid oxidation mediated by Acyl-CoA synthetase long chain 3 is required for mutant KRAS lung tumorigenesis. *Cell Rep.* **16**, 1614–1628 (2016).
66. Traynor-Kaplan, A. et al. Fatty-acyl chain profiles of cellular phosphoinositides. *Biochim. Biophys. Acta* **1862**, 513–522 (2017).

Acknowledgements

We wish to thank J. Sondek for providing the rat PLCγ1 plasmid (UNC Center for Structural Biology, Chapel Hill, USA). The NSCLC cell lines were provided by J. D. Minna (UTSW medical center, USA). We thank A. Traynor-Kaplan (University of Washington, USA) for help with mass spectrometry analysis. We thank G. Ramadori (University of Geneva, Switzerland) for critically reading the manuscript. This study was supported by the German Research Council (DFG; HE6233/4-1 to F.H.H. and SCHN15561-1 to T.M.S.), the Thuringian state program ProExzellenz (RegenerAging-FSU-I-03/14) of the Thuringian Ministry for Research (TMWWDG; to F.H.H.), local funds from the University of Ferrara (FIR-2017), the Italian Ministry of Health (GR-2016-02364602) and the Italian Ministry of Education, University and Research (PRIN Grant 2017XA5J5N) (to A.R.), the Italian Association for Cancer Research (AIRC, IG-18624), Telethon (GGP11139B), the Italian Ministry of Education, University and Research (PRIN Grant 2017E5L5P3), local funds from the University of Ferrara (to P.P.), and the Swiss National Science Foundation (#PP00P3_163929) Professorship (to G.K.).

Author contributions

G.K. and M.S. conceived and designed the experiments. M.S., M.R.S., C.P. and G.K. performed and analysed the data. F.H.H. and T.M.S. generated and provided the *Plcg1*$^{fl/fl}$ mice. S.S.P., L.B. and S.A.B. (pathologists) and R.S. (surgeon) provided the human lung tissue samples, and S.A.B. performed the PLCγ1 staining grading. A.R. and P.P. performed the Ca^{2+} measurements. J.B. and S.F. performed the Seahorse experiments. G.K. supervised the study. G.K. and M.S. wrote the manuscript.

Competing interests

The authors declare no competing interests.

Additional information

Extended data is available for this paper at https://doi.org/10.1038/s41556-020-00592-8.

Supplementary information is available for this paper at https://doi.org/10.1038/s41556-020-00592-8.

Correspondence and requests for materials should be addressed to G.K.

Reprints and permissions information is available at www.nature.com/reprints.

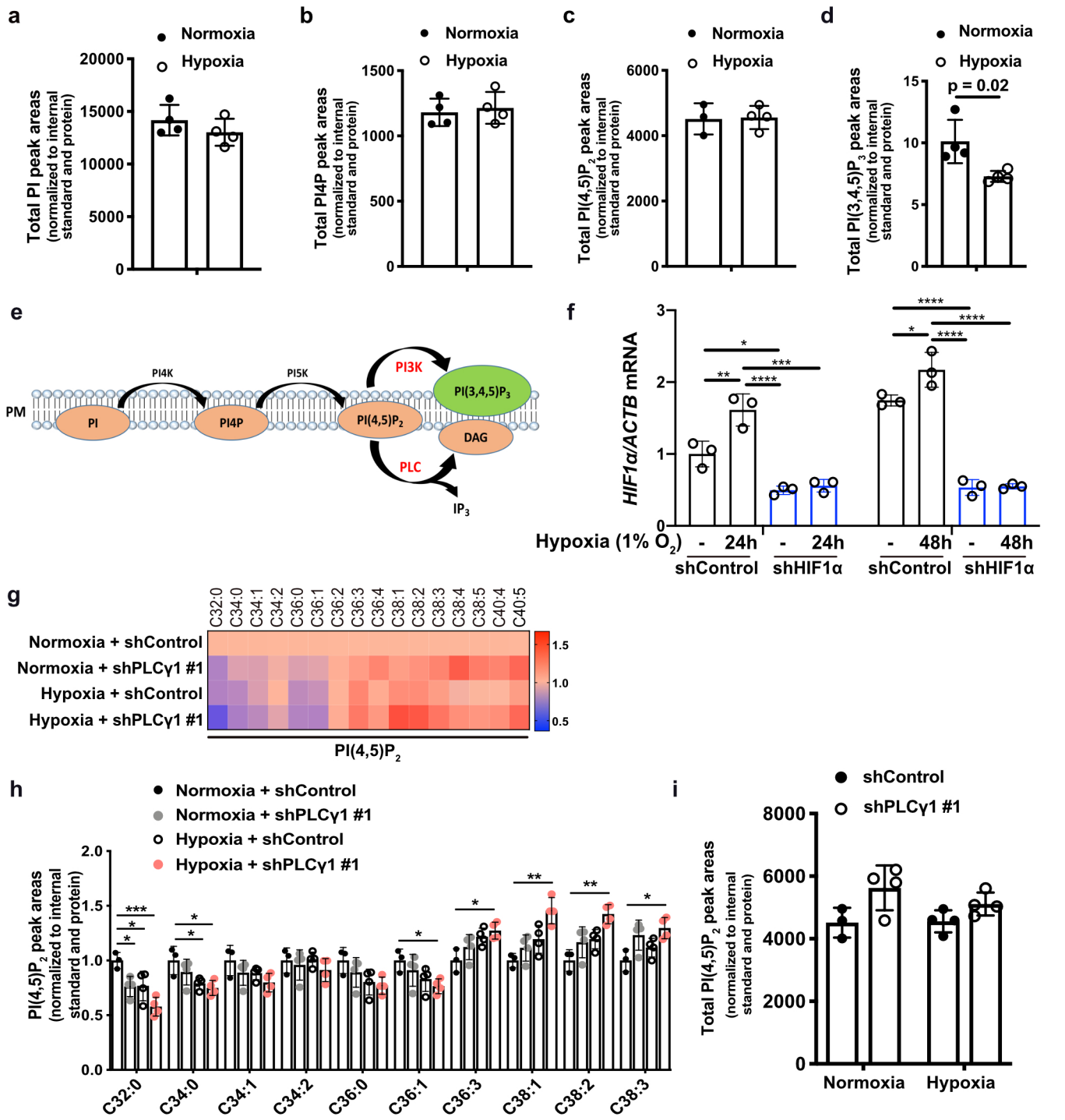

Extended Data Fig. 1 | Hypoxia suppresses PLCγ1 and alters the fatty acid composition of phosphoinositides. a-d, Total PI (**a**), PI4P (**b**), PI(4,5)P_2 (**c**) and PI(3,4,5)P_3 (**d**) peak areas of A549 cells in normoxia and upon shift to hypoxia (1% O_2) for 48h measured by ultra-performance liquid chromatography - tandem mass spectrometry; n = 4/group. **e**, Schematic representation of phosphoinositol signalling and the metabolic fate of PI(4,5)P_2. PM: plasma membrane. PI: phosphatidylinositol, PI4P: phosphatidylinositol-4-phosphate, PtdIns(4,5)P_2: phosphatidylinositol-4,5-biphosphate, PI(3,4,5)P_3: phosphatidylinositol-3,4,5-trisphosphate. **f**, *HIF1a* mRNA expression level in A549 cells (relative to normoxia control at 24h). Cells were transduced with either an empty vector (Tet-pLKO-puro, shControl) or a doxycycline-inducible shRNA against HIF1α and incubated in normoxia or hypoxia for the indicated time; n = 3. **g**, Heatmap display of PI(4,5)P_2 lipid alterations (fold change). A549 cells were transduced with either an empty vector control (Tet-pLKO-puro, shControl) or a doxycycline-inducible shRNA against PLCγ1, treated with doxycycline for 48h and treated as in (**a**); n = 4/group. **h**, Peak areas of the indicated PI(4,5)P_2 lipid species in A549 cells from (**g**); n = 4/group. **i**, Total PI(4,5)P_2 peak areas in A549 cells treated as in (**g**); n = 4/group.All graphical data are presented as mean ± SD. Statistical analyses were done using two-tailed unpaired Student's *t* test or one-way ANOVA; *n*, number of biologically independent samples. * $p < 0.05$, ** $p < 0.01$, *** $p < 0.001$, **** $p < 0.0001$. Statistical source data are provided in Source Data Extended Data Fig. 1.

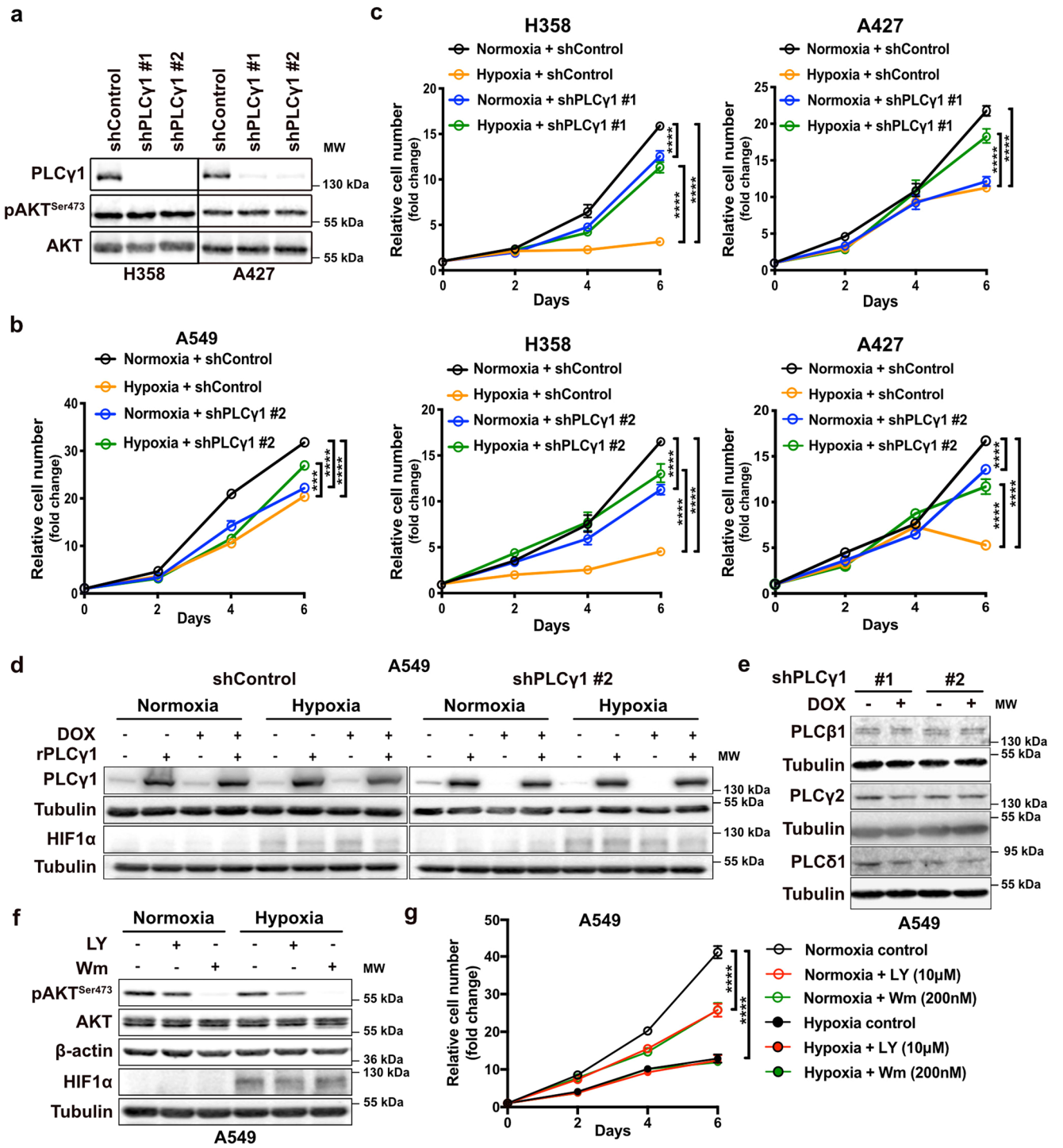

Extended Data Fig. 2 | PLCγ1 suppression promotes cancer cell proliferation during hypoxia. a, Immunoblot analysis of the indicated targets in H358 and A427 cells transduced with either an empty vector control (Tet-pLKO-puro, shControl) or 2 doxycycline-inducible shRNAs against PLCγ1. Cells were incubated in the presence of doxycycline for 72h in normoxia before performing the immunoblot analysis. **b**,**c**, Relative cell number of A549, H358 and A427 cells transduced with either an empty vector control (Tet-pLKO-puro, shControl), or a doxycycline-inducible shRNA against PLCγ1 (as indicated). After this, cells were plated and incubated for the indicated time in normoxia or hypoxia; n = 3. **d**, Immunoblot analysis of the indicated targets in A549 cells transduced as in (**b**). Cells were then incubated in the presence of doxycycline and transfected with either pcDNA3.1 empty vector or pcDNA3.1-rPLCγ1 (shRNA-resistant PLCγ1) and incubated for 72h in normoxia or hypoxia. **e**, Immunoblot analysis of the indicated targets in A549 cells transduced as in (**a**). **f**,**g**, Immunoblot analysis of the indicated targets (**f**) and cell proliferation assay (**g**) of A549 cells treated as indicated in normoxia or hypoxia; n = 3.All graphical data are presented as mean ± SD. Statistical analyses were done using one-way ANOVA; *n*, number of biologically independent samples. **** $p < 0.0001$. Statistical source data and unprocessed immunoblots are provided in Source Data Extended Data Fig. 2.

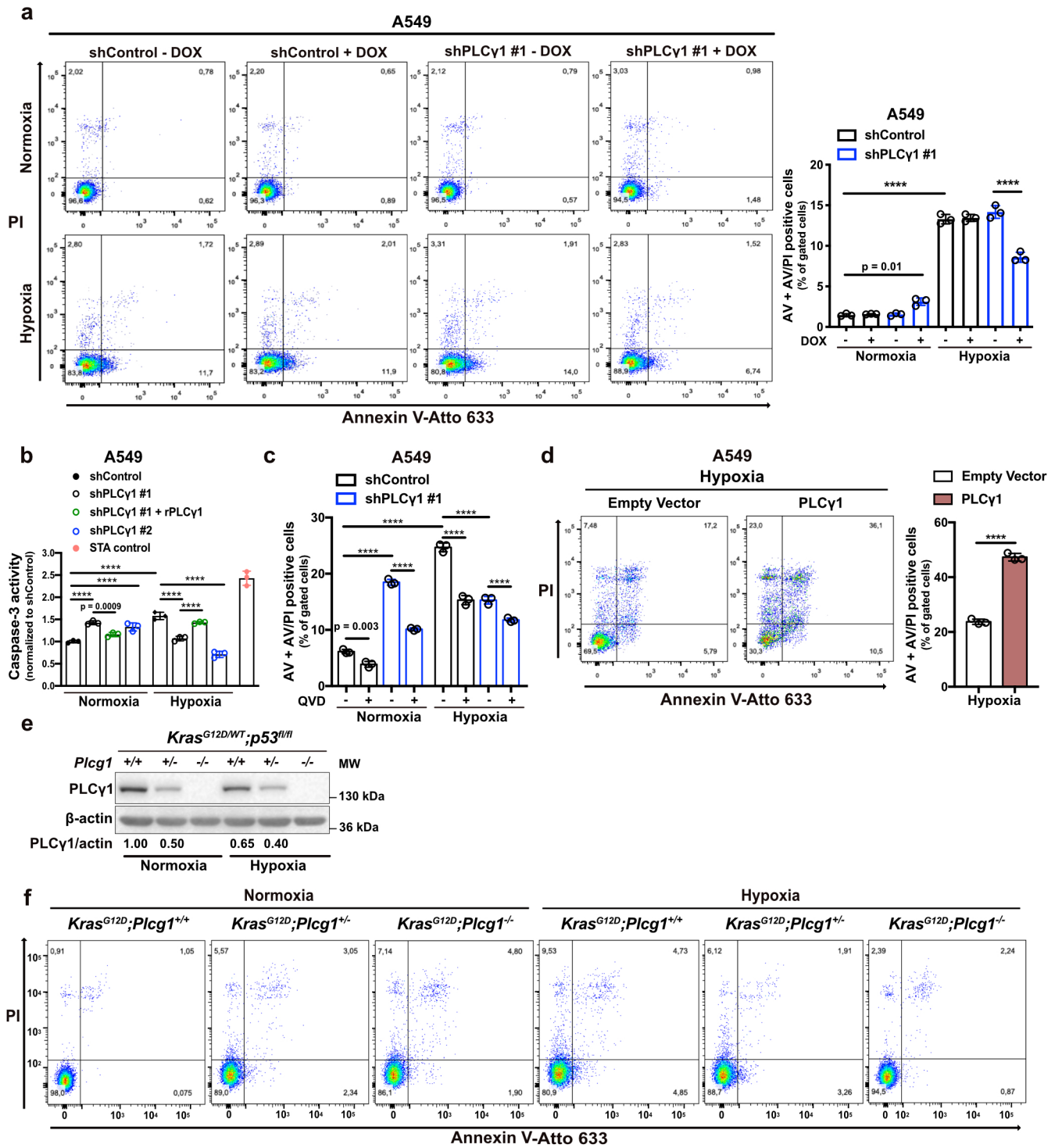

Extended Data Fig. 3 | PLCγ1 suppression promotes cancer cell survival during hypoxia. a, Representative panels of Annexin V-Atto 633/Propidium iodide (PI) flow cytometry analysis (left) and relative quantification of Annexin V (AV) + Annexin V/PI (AV/PI)-positive cells (right) in A549 cells transduced with either an empty vector control (Tet-pLKO-puro, shControl) or a doxycycline-inducible shRNA against PLCγ1, incubated without/with doxycycline for 48h and moved in normoxia or hypoxia for 72h; n = 3. **b**, Caspase-3 activity assay in A549 cells transduced as in (**a**). Cells were then transfected with either pcDNA3.1 empty vector or pcDNA3.1-rPLCγ1 (shRNA-resistant PLCγ1), and incubated in normoxia or hypoxia for 48h. Staurosporine (STA, 100nM) is positive control of caspase-dependent death; n = 3. **c**, Quantification of Annexin V (AV) + Annexin V/PI (AV/PI)-positive cells by flow cytometry in A549 cells transduced as in (**a**). Cells were then treated with Q-VD-OPH (QVD), a pan-caspase inhibitor for 24h; n = 3. **d**, Representative panels of Annexin V-Atto 633/Propidium iodide (PI) flow cytometry analysis (left) and relative quantification of Annexin V (AV) + Annexin V/PI (AV/PI)-positive cells (right) in A549 cells transduced with either pcDNA3.1 empty vector or pcDNA3.1-PLCγ1 and incubated in hypoxia for 72h; n = 3. **e**, Immunoblot analysis of the indicated targets in MEF cells with the indicated genotype in normoxia or hypoxia. The samples derive from the same experiment and the gel/blot were processed in parallel. **f**, Representative panels of Annexin V-Atto 633/Propidium iodide (PI) flow cytometry analysis of MEF cells with the indicated genotype. Graphical data are mean ± SD. Statistical analyses were done using two-tailed unpaired Student's *t* test or one-way ANOVA; *n*, number of biologically independent samples. **** $p < 0.0001$. Statistical source data and unprocessed immunoblots are provided in Source Data Extended Data Fig. 3.

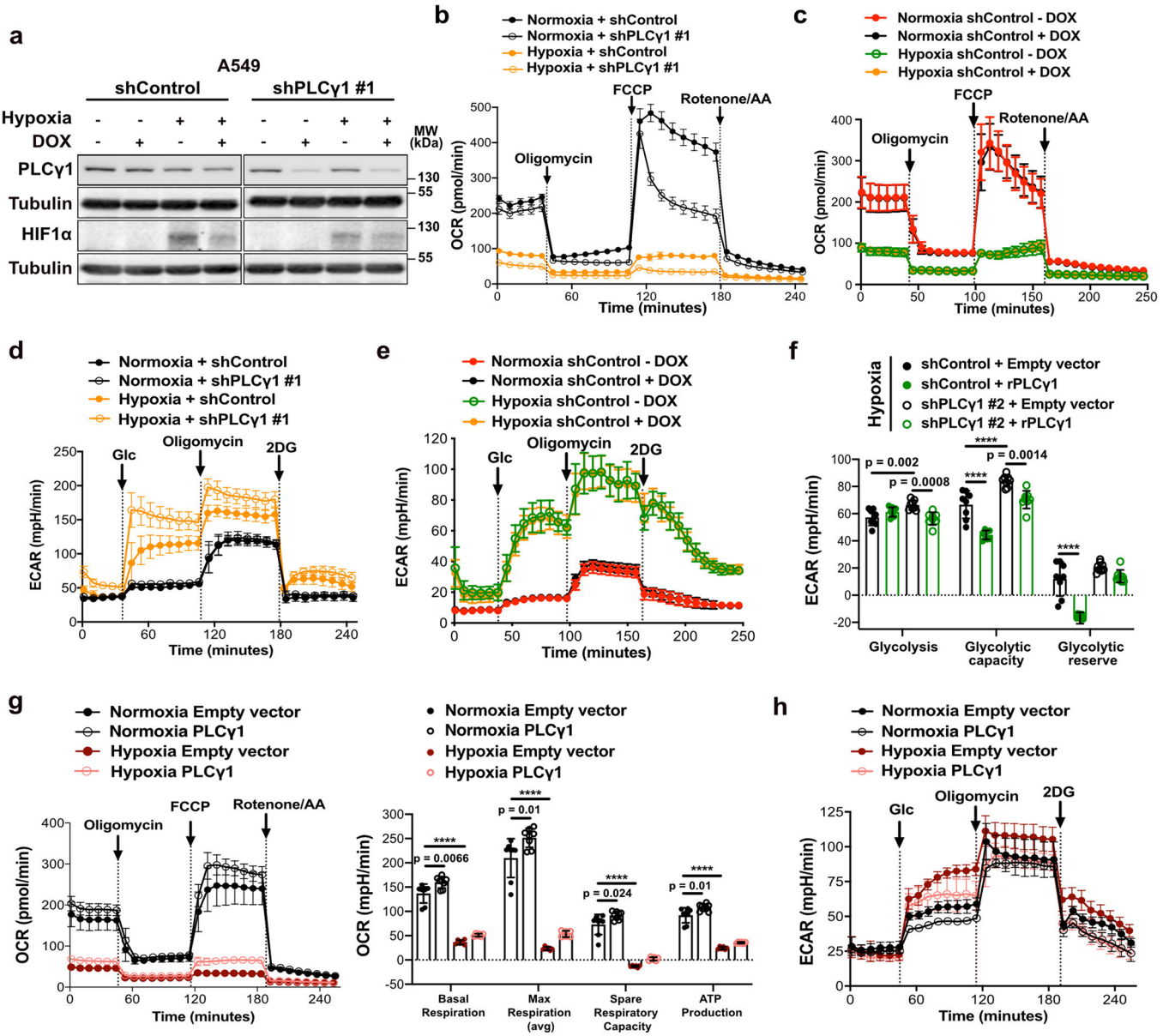

Extended Data Fig. 4 | PLCγ1 suppression decreases mitochondrial respiration and enhances cancer cell glycolytic capacity in human NSCLC cells. a, Immunoblot analysis of the indicated targets in A549 cells transduced with either an empty vector control (Tet-pLKO-puro, shControl) or a doxycycline-inducible shRNA against PLCγ1, incubated without/with doxycycline for 48h and further incubated for 48h in normoxia or hypoxia (3% O_2). **b-e**, Graphs showing oxygen consumption rate (OCR, **b** and **c**) and extracellular acidification rate (ECAR, d and e) of A549 cells transduced and treated as in (**a**); n replicates/group: (**b**) = 8, (**c**) = 7 normoxia/8 hypoxia, (**d**) = 9 normoxia/ 8 hypoxia, (**e**) = 8. Panels (c and e) are treated without/with doxycycline and serve as a control for the doxycycline effect on cells. **f**, Bar graph showing ECAR parameters in A549 cells transduced as in (**a**). Cells were transfected with either pcDNA3.1 empty vector or pcDNA3.1-rPLCγ1 (shRNA-resistant PLCγ1) to rescue the shPLCγ1 #2 and incubated for 48h in normoxia or hypoxia; n = 8. **g-h**, Oxygen consumption rate (**g**) and extracellular acidification rate (**h**) parameters of A549 cells transfected with either pcDNA3.1 empty vector or pcDNA3.1-PLCγ1 and incubated for 48h in normoxia or hypoxia; (**g**) n = 8 for normoxia and 6 for hypoxia groups, (**h**) n = 7.OCR was determined during sequential treatments with oligomycin, FCCP and rotenone/antimycin (AA). ECAR was determined during sequential treatments with glucose (Glc), oligomycin and 2 deoxyglucose (2DG).Graphical data are mean ± SD. Statistical analyses were done using one-way ANOVA; *n*, number of biologically independent samples. **** $p < 0.0001$. Statistical source data and unprocessed immunoblots are provided in Source Data Extended Data Fig. 4.

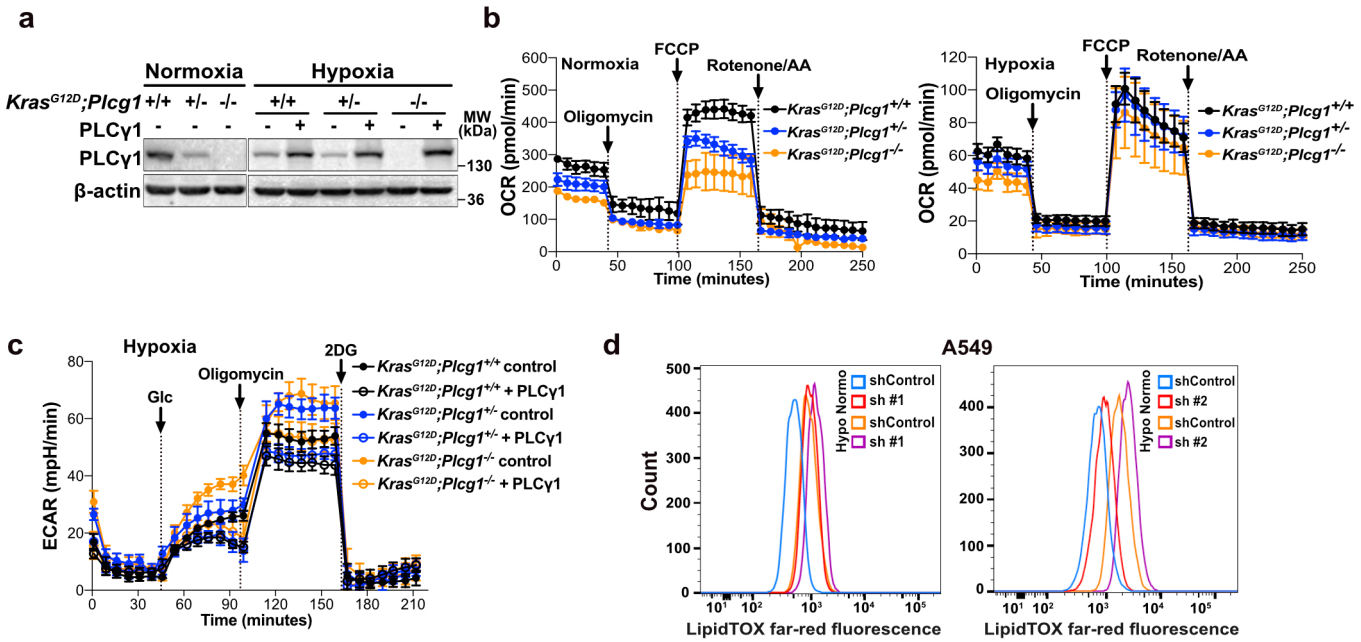

Extended Data Fig. 5 | PLCγ1 suppression decreases mitochondrial respiration and enhances cancer cell glycolytic capacity in MEFs. a, Immunoblot analysis of the indicated targets in MEF cells with the indicated genotype transfected with either pcDNA3.1-HA-LIC empty vector or pcDNA3.1-HA-LIC-PLCγ1. 24h later, cells were moved in hypoxia (3% O_2) and incubated for additional 48h. **b**, Oxygen consumption rate (OCR) graph of MEF cells of the indicated genotypes. Cells were incubated for 48h in normoxia or hypoxia (3% O_2) before seahorse experiment. OCR was determined during sequential treatments (indicated with arrows) with oligomycin, FCCP and rotenone/antimycin (AA) at the indicated time; n = 3 for the normoxia groups and n = 6 for the hypoxia groups. **c**, Graph showing extracellular acidification rate (ECAR) of MEF cells with the indicated genotype transduced as in (**a**). ECAR was determined during sequential treatments (indicated with arrows) with glucose (Glc), oligomycin and 2 deoxyglucose (2DG) at the indicated time; n = 6. **d**, Flow cytometry panels showing mean fluorescent intensity of A549 cells from experiment reported in main Fig. 3i. A549 cells were previously transduced with either an empty vector control (Tet-pLKO-puro, shControl) or 2 different doxycycline-inducible shRNAs against PLCγ1 (shPLCγ1 #1, shPLCγ1 #2), incubated in the presence of doxycycline for 48h, incubated for additional 48h in normoxia or hypoxia (1% O_2), stained with LipidTOX and analyzed by flow cytometry. Sh#1: shPLCγ1 #1, Sh#2: shPLCγ1 #2; n = 3. Graphical data are mean ± SD; *n*, number of biologically independent samples. Statistical source data and unprocessed immunoblots are provided in Source Data Extended Data Fig. 5.

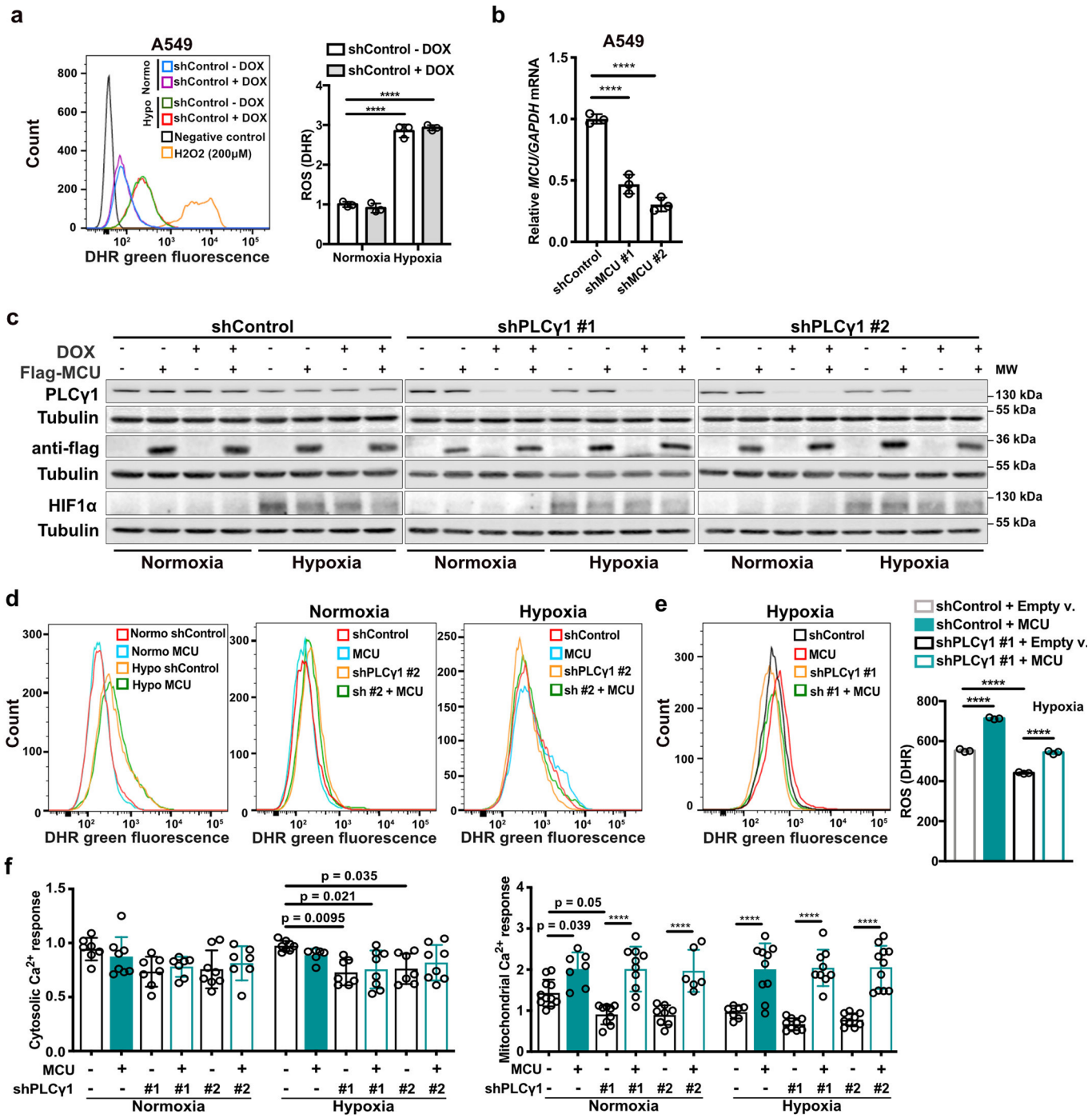

Extended Data Fig. 6 | PLCγ1 suppression depletes mitochondrial ROS through impairment of Ca^{2+} entry into the mitochondria. a, Flow cytometry histograms (left) and quantification of DHR (green, right) of A549 cells transduced with an empty vector (Tet-pLKO-puro, shControl) and incubated without/with doxycycline (DOX) for 48h, incubated for additional 48h in normoxia or hypoxia and stained with DHR for flow-cytometry. H_2O_2: positive control. DHR: Dihydrorhodamine. Normo: normoxia. Hypo: hypoxia. n = 3. **b**, *MCU* mRNA levels in A549 cells transduced with an empty vector (Tet-pLKO-puro, shControl) or 2 doxycycline-inducible shRNAs against MCU and incubated with doxycycline for 72h; n = 3. **c**, Immunoblot analysis of the indicated targets in A549 cells transduced with an empty vector (Tet-pLKO-puro, shControl) or 2 doxycycline-inducible shRNA against PLCγ1, transfected with either pcDNA3.1 empty vector or pcDNA3.1-MCU-flag plasmid and incubated in normoxia or hypoxia for 48h. **d**, Representative flow cytometry histograms of DHR (green) mean fluorescent intensity of A549 cells from experiment reported in main Fig. 4f. Sh#2: shPLCγ1 #2. **e**, Representative flow cytometry histograms (left) and quantification of DHR (green) of A549 cells transduced with an empty vector (Tet-pLKO-puro, shControl) or a doxycycline-inducible shRNA against PLCγ1. Cells were then treated with doxycycline for 24h, transfected with either pcDNA3.1 empty vector or pcDNA3.1-MCU-flag plasmid and moved to hypoxia for additional 48h before staining cells with DHR for analysis. DHR: Dihydrorhodamine. Sh#1: shPLCγ1 #1; n = 3. **f**, Cytosolic (left) and mitochondrial (right) Ca^{2+} response of A549 cells transduced as in (**c**), transfected with appropriate targeted-aequorin and histamine-induced Ca^{2+} was measured 48h after incubation in normoxia or hypoxia; n/group = cytosolic normoxia 7, 8, 7, 7, 8, 7/cytosolic hypoxia 8, 6, 7, 8, 7, 8. n/group = mitochondrial normoxia 11, 7, 9, 10, 8, 6/mitochondrial hypoxia 7, 10, 9, 9, 9, 11.Graphical data are mean ± SD. Statistical analyses were done using one-way ANOVA; *n*, number of biologically independent samples. **** $p < 0.0001$. Statistical source data and unprocessed immunoblots are provided in Source Data Extended Data Fig. 6.

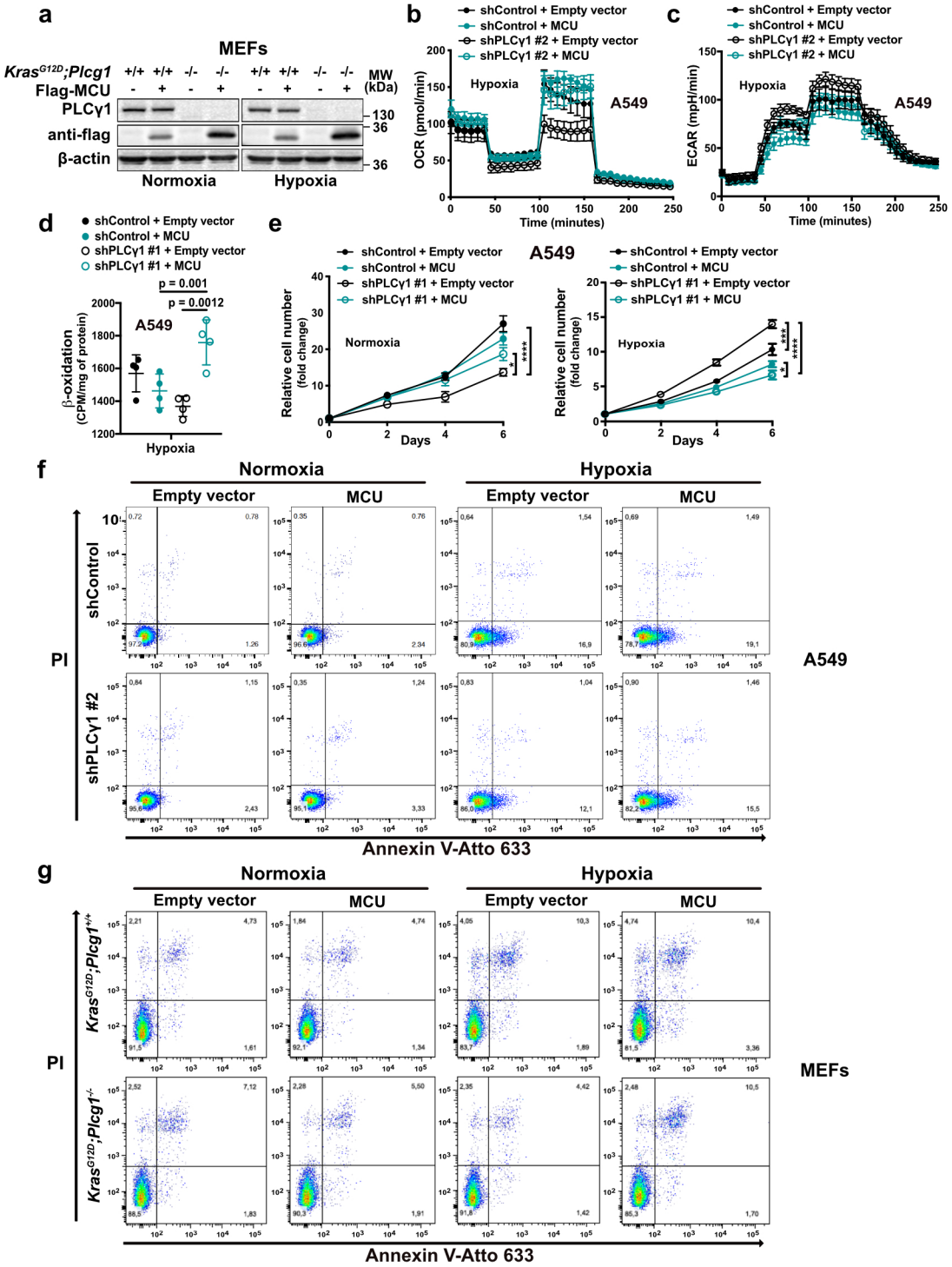

Extended Data Fig. 7 | PLCγ1 suppression enhances cell proliferation and decreases cell death in hypoxia through impairment of Ca^{2+} entry into the mitochondria. a, Immunoblot analysis of the indicated targets in MEFs generated from a *LSL-Kras$^{G12D/WT}$;p53$^{flox/flox}$;Plcg1$^{wt/wt}$* and *LSL-Kras$^{G12D/WT}$;p53$^{flox/flox}$;Plcg1$^{flox/flox}$* mouse model, stably transduced with Cre recombinase (pMSCV-hygro-Cre) and transfected with either pcDNA3.1 empty vector or pcDNA3.1-MCU-flag plasmid and moved to hypoxia (1% O_2) for additional 48h. **b**,**c**, Oxygen consumption rate (**b**) and extracellular acidification rate (**c**) of A549 cells transduced with either an empty vector (Tet-pLKO-puro, shControl) or a doxycycline-inducible shRNA against PLCγ1, treated with doxycycline for 24h, transfected with either pcDNA3.1 empty vector or pcDNA3.1-MCU-flag plasmid and incubated for 48h in hypoxia (3% O_2). OCR was determined during sequential treatments (indicated with arrows) with oligomycin, FCCP and rotenone/antimycin (AA) at the indicated time. ECAR was determined during sequential treatments (indicated with arrows) with glucose (Glc), oligomycin and 2 deoxyglucose (2DG) at the indicated time; n = 5. **d**, Fatty acid β-oxidation of A549 cells transduced and treated as in (**b**); n = 4. **e**, Relative cell number of A549 cells transduced and treated as in (**b**); n = 3. Normoxia: $^{*}p = 0.03$, hypoxia: $^{*}p = 0.014$, $^{***}p = 0.0005$. **f**, Representative Annexin V-Atto 633/Propidium iodide (PI) flow cytometry analysis panels of A549 cells from experiment reported in main Fig. 5e; n = 3. **g**, Representative Annexin V-Atto 633/Propidium iodide (PI) flow cytometry analysis panels of MEF cells from experiment reported in main Fig. 5f; n = 3. Graphical data are mean ± SD. Statistical analyses were done using one-way ANOVA; *n*, number of biologically independent samples. $^{****}p < 0.0001$. Statistical source data and unprocessed immunoblots are provided in Source Data Extended Data Fig. 7.

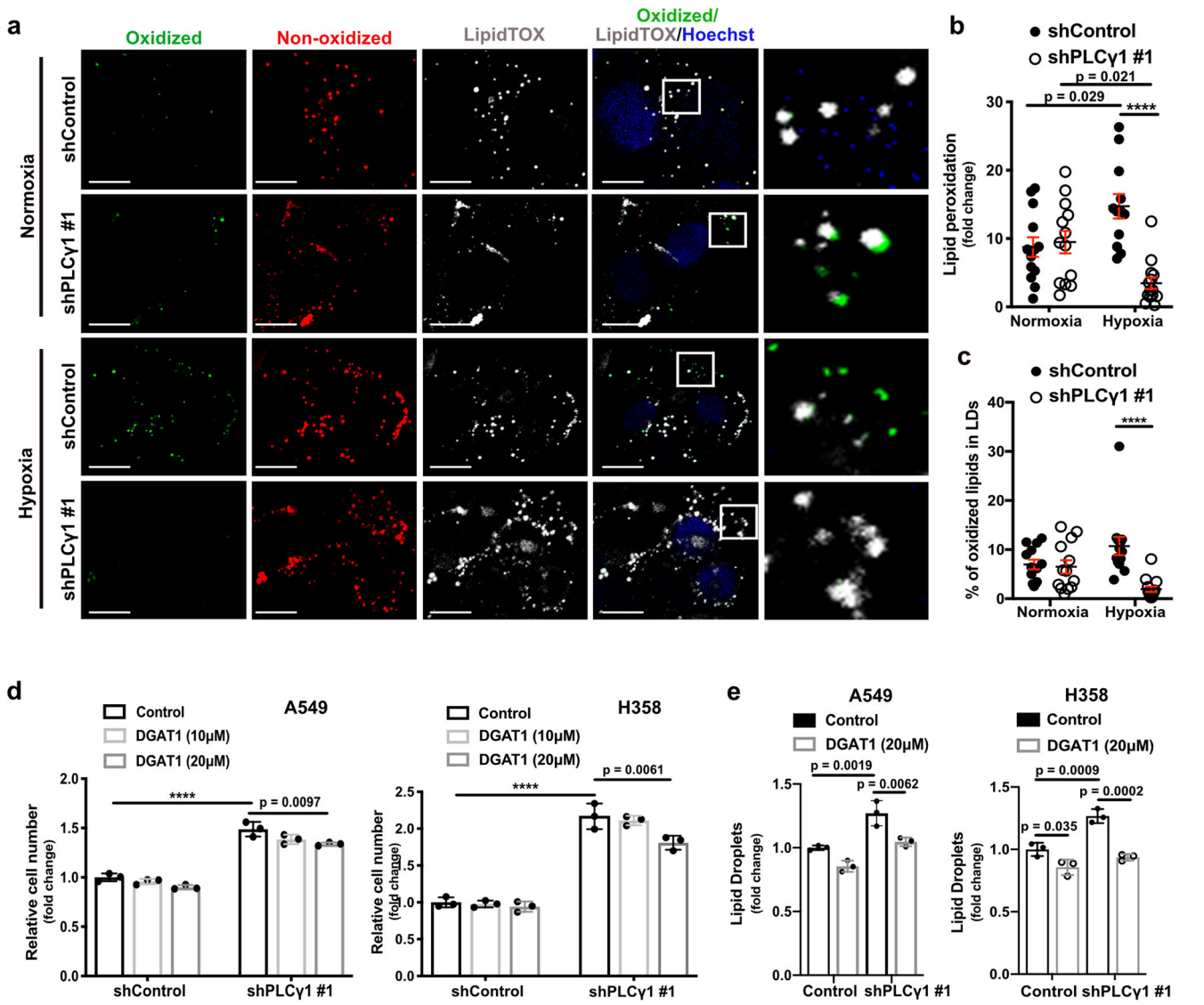

Extended Data Fig. 8 | PLCγ1 suppression reduces hypoxia-induced lipid peroxidation. a, Confocal microscopy of A549 cells transduced with either an empty vector (Tet-pLKO-puro, shControl) or a doxycycline-inducible shRNA against PLCγ1 (shPLCγ1 #1) and incubated in the presence of doxycycline for 48h. Cells were then incubated for 48h in normoxia or hypoxia (1% O_2), stained with BODIPY 581/591 C11 (green: oxidized lipids / red: non-oxidized lipids), LipidTOX (grey) to mark lipid droplets and Hoechst (nuclei). White squares represent magnified areas on the right. Scale bars: 20 μm. **b**, Quantification of lipid peroxidation expressed as percent of oxidized lipids from (**a**); n/group = 13, 13, 12, 14. **c**, Quantification of oxidized lipids, expressed as percent, localized in lipid droplets from (**a**); n/group = 13, 13, 13, 14. **d**, Relative cell number of A549 (left) and H358 (right) cells transduced with either an empty vector (Tet-pLKO-puro, shControl) or a doxycycline-inducible shRNA against PLCγ1 (shPLCγ1 #1), incubated with doxycycline for 48h and treated as indicated with the DGAT1 inhibitor (T863). The graphs represent day 6 of the cell proliferation assay; n = 3. **e**, Lipid droplet quantification (relative to control) of A549 and H358 cells treated as in (**d**), stained with LipidTOX (far red) and analyzed by flow cytometry; n = 3.Graphical data are mean ± SD except the panels b and c that are mean ± SEM. Statistical analyses were done using one-way ANOVA; *n*, number of biologically independent samples. **** $p < 0.0001$. Statistical source data are provided in Source Data Extended Data Fig. 8.

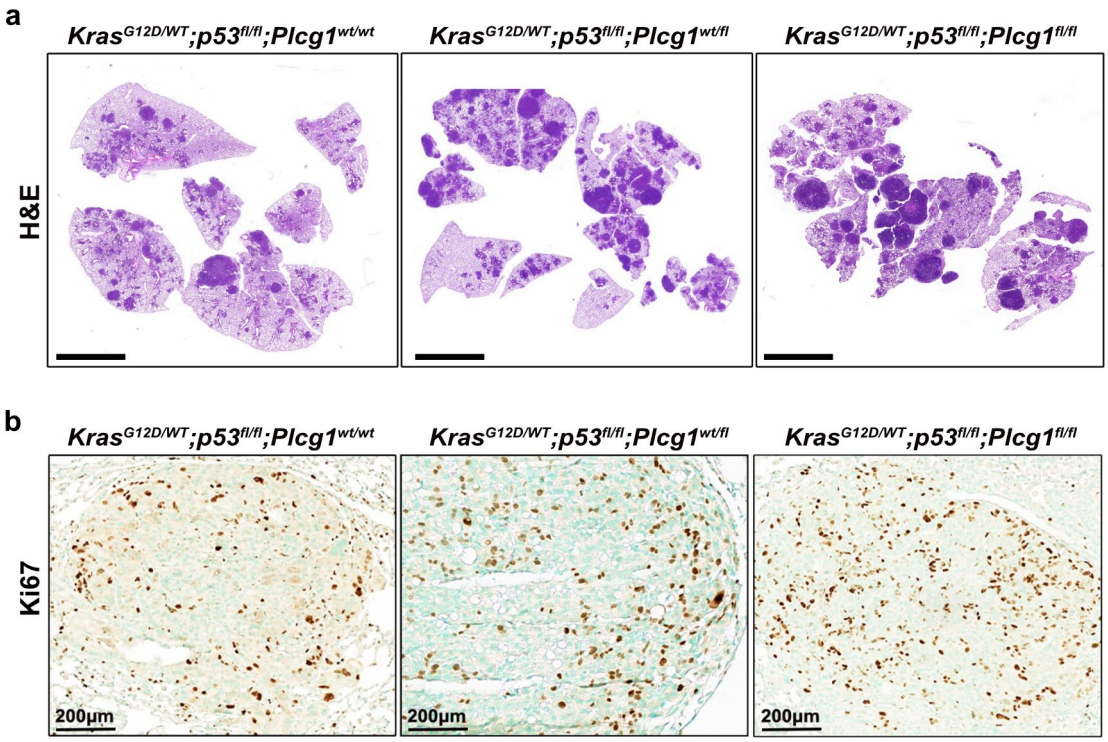

Extended Data Fig. 9 | PLCγ1 deletion accelerates lung tumorigenesis in mice. a, Representative hematoxylin & eosin (H&E) staining of *LSL-Kras*$^{G12D/WT}$;*p53*$^{flox/flox}$;*Plcg1*$^{wt/wt}$, *LSL-Kras*$^{G12D/WT}$;*p53*$^{flox/flox}$;*Plcg1*$^{wt/flox}$ and *LSL-Kras*$^{G12D/WT}$;*p53*$^{flox/flox}$;*Plcg1*$^{flox/flox}$ mouse lung sections, 10 weeks after Cre induction. Scale bar: 5000μm. **b**, Representative immunohistochemistry images showing Ki67-positive cell staining in mouse lung tumors from *LSL-Kras*$^{G12D/WT}$;*p53*$^{flox/flox}$;*Plcg1*$^{wt/wt}$, *Kras*$^{G12D/WT}$;*p53*$^{flox/flox}$;*Plcg1*$^{wt/flox}$ and *LSL-Kras*$^{G12D/WT}$;*p53*$^{flox/flox}$;*Plcg1*$^{flox/flox}$ mice 10 weeks after Cre induction. This is related to main Fig. 7e.

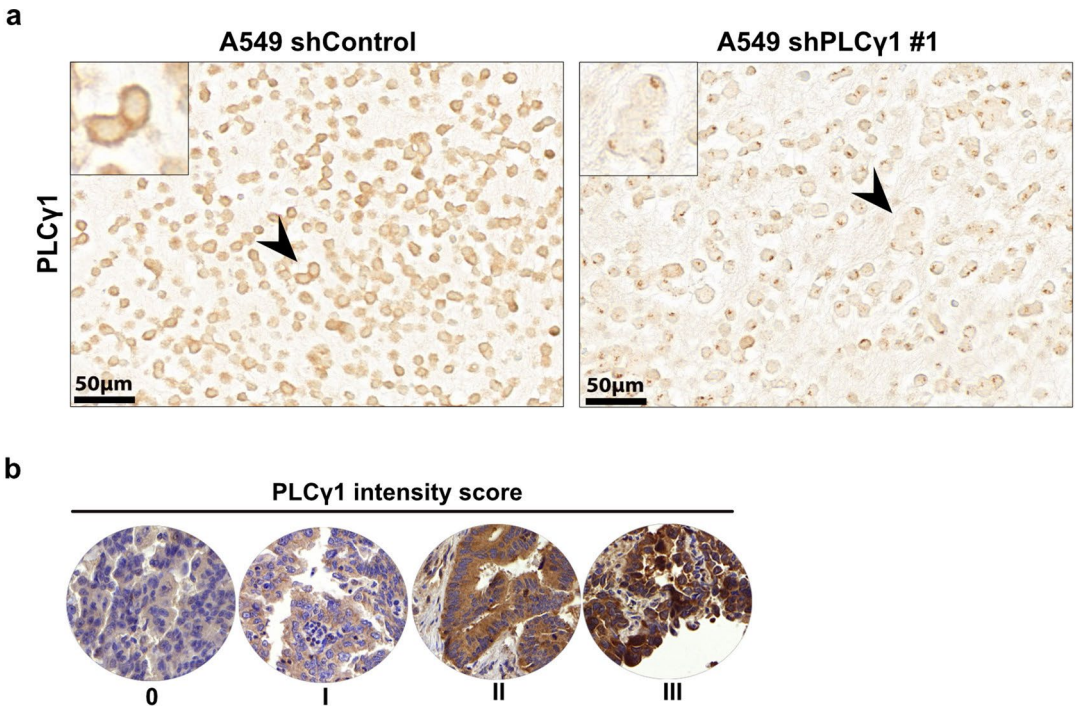

Extended Data Fig. 10 | Low PLCγ1 levels in human lung adenocarcinomas correlate with poor patient survival. a, Antibody validation for IHC against PLCγ1 on human tumor tissue microarray. A549 cells previously transduced with either an empty vector (Tet-pLKO-puro, shControl) or a doxycycline-inducible shRNA against PLCγ1 (shPLCγ1 #1) and incubated in the presence of doxycycline for 48h before paraffin embedding. Subsequently IHC was performed as for TMA staining (described in materials and methods). The arrow heads indicate PLCγ1-positive cells shown at higher magnification in the inset **b**, Representative images of the human lung adenocarcinoma TMA showing the staining intensity with the matched scoring by the pathologist upon immunohistochemistry against PLCγ1. Score 0-I was considered low staining intensity, II was considered moderate and score III was considered high staining intensity.

nature research

Corresponding author(s): Georgia Konstantinidou

Last updated by author(s): Aug 13, 2020

Reporting Summary

Nature Research wishes to improve the reproducibility of the work that we publish. This form provides structure for consistency and transparency in reporting. For further information on Nature Research policies, see Authors & Referees and the Editorial Policy Checklist.

Statistics

For all statistical analyses, confirm that the following items are present in the figure legend, table legend, main text, or Methods section.

n/a	Confirmed	
☐	☒	The exact sample size (*n*) for each experimental group/condition, given as a discrete number and unit of measurement
☐	☒	A statement on whether measurements were taken from distinct samples or whether the same sample was measured repeatedly
☐	☒	The statistical test(s) used AND whether they are one- or two-sided *Only common tests should be described solely by name; describe more complex techniques in the Methods section.*
☒	☐	A description of all covariates tested
☐	☒	A description of any assumptions or corrections, such as tests of normality and adjustment for multiple comparisons
☐	☒	A full description of the statistical parameters including central tendency (e.g. means) or other basic estimates (e.g. regression coefficient) AND variation (e.g. standard deviation) or associated estimates of uncertainty (e.g. confidence intervals)
☐	☒	For null hypothesis testing, the test statistic (e.g. *F*, *t*, *r*) with confidence intervals, effect sizes, degrees of freedom and *P* value noted *Give P values as exact values whenever suitable.*
☒	☐	For Bayesian analysis, information on the choice of priors and Markov chain Monte Carlo settings
☒	☐	For hierarchical and complex designs, identification of the appropriate level for tests and full reporting of outcomes
☒	☐	Estimates of effect sizes (e.g. Cohen's *d*, Pearson's *r*), indicating how they were calculated

Our web collection on statistics for biologists contains articles on many of the points above.

Software and code

Policy information about availability of computer code

Data collection	GUI Xenabrowser, Li-Cor fluorescence-chemiluminescence detector, Pannoramic Midi II digital slide scanner .
Data analysis	QuPath v.0.1.2, Imaris Image Analysis Software v.9.5.1, FlowJo V10, GraphPad Prism v.7

For manuscripts utilizing custom algorithms or software that are central to the research but not yet described in published literature, software must be made available to editors/reviewers. We strongly encourage code deposition in a community repository (e.g. GitHub). See the Nature Research guidelines for submitting code & software for further information.

Data

Policy information about availability of data

All manuscripts must include a data availability statement. This statement should provide the following information, where applicable:

- Accession codes, unique identifiers, or web links for publicly available datasets
- A list of figures that have associated raw data
- A description of any restrictions on data availability

All Source data for Figs. 1-8 and and Extended Data Figs. 1-10 are included in this published article (and in its Extended Data files, Supplementary Fig. 1 and Supplementary Tables 1 and 2). Requests to use the PLCγ1 floxed mice will be redirected to Florian H. Heidel and Tina M. Schnöder. The Cancer Genome Atlas (TCGA) lung adenocarcinoma (LUAD) dataset was retrieved from the Genomic Data Commons Portal: http://cancergenome.nih.gov. The data were downloaded with the help of the web graphic user interface Xena browser https://xenabrowser.net.

Field-specific reporting

Please select the one below that is the best fit for your research. If you are not sure, read the appropriate sections before making your selection.

☒ Life sciences ☐ Behavioural & social sciences ☐ Ecological, evolutionary & environmental sciences

For a reference copy of the document with all sections, see nature.com/documents/nr-reporting-summary-flat.pdf

Life sciences study design

All studies must disclose on these points even when the disclosure is negative.

Sample size	For in vivo mouse experiments, we used G* Power probability and set to 5% the significance level, to determine the number of mice necessary. For all in vitro experiments we typically used at least 3 independent cell cultures per condition and the experiments were repeated at least 2-3 times with similar results.
Data exclusions	No data were excluded from analyses.
Replication	Biological replicates in each experiment are defined in the figure legends. Experiments have been reproduced at least 3 times as stated in the methods section "Statistics and Reproducibility" except for the MS-based lipidomics that was performed twice. Studies involving mice were typically performed once to limit the use of animals, unless indicated otherwise. However, several tumor models and mouse strains were employed to validate the robustness of key results in different biological systems.
Randomization	No specific method of randomization was used for the in vitro experiments. All the mouse experiments were randomized. Animals were first genotyped and then males were randomly assigned to each group after balancing of age.
Blinding	Blinded studies were carried on for seahorse experiments, ultra performance liquid chromatography - tandem mass spectrometry and microscopy-based quantifications (determination of lipid droplet size and number, quantification of pimonidazole-related stainings) and TMA scoring. Blinding in mouse studies was not possible due to tagging of the mice and access to identification codes by the investigators. Thus, although data acquisition was blinded in most cases samples were labeled with identification codes and the investigators had access to the identity of the samples through the identification codes.

Reporting for specific materials, systems and methods

We require information from authors about some types of materials, experimental systems and methods used in many studies. Here, indicate whether each material, system or method listed is relevant to your study. If you are not sure if a list item applies to your research, read the appropriate section before selecting a response.

Materials & experimental systems

n/a	Involved in the study
☐	☒ Antibodies
☐	☒ Eukaryotic cell lines
☒	☐ Palaeontology
☐	☒ Animals and other organisms
☐	☒ Human research participants
☒	☐ Clinical data

Methods

n/a	Involved in the study
☒	☐ ChIP-seq
☐	☒ Flow cytometry
☒	☐ MRI-based neuroimaging

Antibodies

Antibodies used

Rabbit polyclonal Anti-phospho-PLCγ1 (Tyr783) (WB, 1:1000) Cell Signaling Technology Cat#2821S, Lot: 9, RRID:AB_330855
Recombinant Monoclonal Rabbit Anti-phospho-PLCγ1 (Tyr783) (1016D) (IF, 10µg/ml) R&D Systems Cat#MAB74542, Lot: CJQJ031901A
Mouse monoclonal Anti-PLCγ1 (E-12) (WB, 1:1000/ IHC, 1:250/human TMA: 1/200) Santa Cruz Biotechnology, Cat#sc-7290, Lot: J1317, RRID:AB_628119
Rabbit monoclonal Anti-PLCγ1 (D9H10) (IHC-F mouse tissue: 1/100) Cell Signaling Technology Cat#5690T, Lot: 1, RRID:AB_10691383
Mouse monoclonal Anti-phospho-PLCγ1 (Tyr783.27) (IHC-F mouse tissue: 1/250) Santa Cruz Biotechnology Cat#sc-136186, Lot: J1617, RRID:AB_2163561
Mouse monoclonal Anti-phospho-PLCβ1 (D-8) (WB, 1:1000) Santa Cruz Biotechnology Cat#sc-5291, Lot: J2617, RRID:AB_628118
Mouse monoclonal Anti-phospho-PLCγ2 (B-10) (WB, 1:1000) Santa Cruz Biotechnology Cat#sc-5283, Lot: L0817, RRID:AB_628120
Mouse monoclonal Anti-phospho-PLCδ1 (D-7) (WB, 1:1000) Santa Cruz Biotechnology Cat#sc-393464, Lot: A2918, RRID:AB_2716743
Rabbit monoclonal Anti-Phospho-Akt (Ser473) (D9E) (WB, 1:1000) Cell Signaling Technology Cat#4060, Lot: 23, RRID:AB_2315049
Mouse monoclonal Anti-AKT (pan) (40D4) (WB, 1:1000) Cell Signaling Technology Cat#2920, Lot: 3, RRID:AB_1147620

Rabbit polyclonal Anti-ADRP (WB/IHC-F/IF, 1:1000) Invitrogen Cat#PA5-79830, Lot: UJ2864087, RRID:AB_2746945
Mouse monoclonal Anti-FAK (H-1) (IF, 1:250) Santa Cruz Biotechnology Cat#sc-1688, Lot: L0817, RRID:AB_627576
Rabbit monoclonal Anti-RAS (27H5) (WB: 1/1000) Cell Signaling Technology, Cat#3339, Lot: 5, RRID:AB_2269641
Rabbit monoclonal Anti-HIF1α (EP1215Y) (WB: 1/1000) Abcam, Cat#ab51608, Lot: GR244245-52, RRID:AB_880418
Purified Mouse Anti-p21 (WB, 1:1000) BD Pharmingen Cat#556430, Lot: 8305560, RRID:AB_396414
Mouse monoclonal Anti-FLAG® (M5) (WB, 1:5000), Sigma-Aldrich Cat#F4042, RRID:AB_439686
Mouse monoclonal Anti-β-actin (AC-74) (WB, 1:2000) Sigma-Aldrich Cat#a-5316, RRID:AB_476743
α-tubulin (WB, 1:2000) Sigma-Aldrich Cat#T6199, RRID:AB_477583
Rabbit monoclonal Anti-Ki-67 (SP6) (IHC, 1:300) Thermo Scientific Cat#RM-9106, RRID:AB_2335745
Mouse monoclonal Anti-pimonidazole (4.3.11.3) (IHC-F, 1:100) Hypoxyprobe™ Cat#HP6-200, Lot: 08.24.18, RRID:AB_2801307
Rabbit polyclonal Anti-pimonidazole (IHC-F: 1/100), Hypoxyprobe™ Cat#HP-FITC Pab1, Lot: 02/15/20
Goat Anti-mouse Green IRDye 800 CW (WB, 1:10000) LI-COR, Cat#926-32210, Lot: C70919-05, RRID:AB_621842
Goat Anti-mouse Red IRDye 680 RD (WB, 1:10000) LI-COR, Cat#926-68070, Lot: 80307-05, RRID:AB_10956588
Goat Anti-rabbit Green IRDye 800 CW (WB, 1:10000) LI-COR, Cat#926-32211, Lot: C60607-15, RRID:AB_621843
Goat Anti-rabbit Red IRDye 680 RD (WB, 1:10000) LI-COR, Cat#926-68071, Lot: C71214-05, RRID:AB_10956166
Amersham ECL Mouse IgG, HRP-linked whole Ab (WB, 1:10000) GE Healthcare Life Sciences Cat#NA931, Lot: 17002495, RRID:AB_772210
Amersham ECL Rabbit IgG, HRP-linked whole Ab (WB, 1:10000) GE Healthcare Life Sciences Cat#NA934, Lot: 16976257, RRID:AB_772206
Alexa Fluor 488 donkey Anti-rabbit (IHC-F, 1:500) Thermo Scientific Cat#A21206, Lot: 1927937, RRID:AB_141708
Alexa Fluor 594 donkey Anti-rabbit (IHC-F, 1:500) Thermo Scientific Cat#A21207, Lot: 1938375, RRID:AB_141637
Alexa Fluor 488 goat Anti-mouse (IHC-F, 1:500) Thermo Scientific Cat#A21121, Lot: 1964382, RRID:AB_141514
Alexa Fluor 594 goat Anti-mouse (IHC-F, 1:500) Thermo Scientific Cat#A21135, Lot: 1850119, RRID:AB_2535774
ImmPRESS® HRP Anti-Rabbit IgG (Peroxidase) Vector Cat#MP-7401, Lot: ZE0306, RRID:AB_2336529
Mouse on Mouse (M.O.M.®) Blocking Reagent Vector Cat#MKB-2213, Lot: ZG0114, RRID:AB_2336587

Validation

We validated all the key antibodies used in the manuscript. Specific validations were performed for the phospho- and total-PLCγ1 antibodies with specific RNAi-mediated knockdown in cell lines or mice deficient for PLCγ1 (Figure 2: cell lines, Figure 6 mice and Figure 7 humans). The validation of this antibody for use on human TMA is reported in Extended Fig. 10. Antibodies used for microscopy imaging presented same cellular patterns as expected by the manufacturer i.e Recombinant Monoclonal Rabbit Anti-phospho-PLCγ1 (Tyr783) (IF, 10µg/ml) R&D Systems Cat#MAB74542 was present in perinuclear halos as well as plasma membrane contact sites (fig. 1i). Rabbit monoclonal Anti-HIF1α (EP1215Y) (WB: 1/1000) Abcam, Cat#ab51608, RRID:AB_880418 was present only in hypoxic tissue and the antibody was validated with specific RNAi-mediated knockdown in cell lines (Fig. 1h). Rabbit polyclonal anti-ADRP (WB/IHC, 1:1000) Invitrogen Cat#PA5-79830, RRID:AB_2746945 was only present in the periphery of lipid droplets as reported in the datasheet.
For the remaining used antibodies see below:
Mouse monoclonal Anti-phospho-PLCβ1 (D-8) (WB, 1:1000) Santa Cruz Biotechnology Cat#sc-5291, RRID:AB_628118. (Shi, Miralles et al. 2016).
Mouse monoclonal Anti-phospho-PLCγ2 (B-10) (WB, 1:1000) Santa Cruz Biotechnology Cat#sc-5283, RRID:AB_628120. The antibody was validated in human cells by Western blot by the manufacturer, showing a single specific band in cells that contain PLCγ2.
Mouse monoclonal Anti-phospho-PLCδ1 (D-7) (WB, 1:1000) Santa Cruz Biotechnology Cat#sc-393464, RRID:AB_2716743. The antibody was validated in human cells by Western blot by the manufacturer, showing a single specific band in cells that contain PLCδ1.
Rabbit monoclonal Anti-Phospho-Akt (Ser473) (D9E) (WB, 1:1000) Cell Signaling Technology Cat#4060, RRID:AB_2315049. The antibody was validated in human cells by Western blot in this manuscript, after treatment of cells with LY294002 (LY) and Wortmannin (Wm), two PI3K inhibitors (Reported in Extended Data Fig. 2f).

Mouse monoclonal Anti-AKT (pan) (40D4) (WB, 1:1000) Cell Signaling Technology Cat#2920, RRID:AB_1147620. The antibody was validated in human cells by Western blot by the manufacturer, showing 2 specific bands.
Rabbit polyclonal Anti-ADRP (WB/IHC-F/IF, 1:1000) Invitrogen Cat#PA5-79830, RRID:AB_2746945. The antibody was validated in human cells by Western blot by the manufacturer, showing a single specific band in cells that contain ADRP.
Mouse monoclonal Anti-FAK (H-1) (IF, 1:250) Santa Cruz Biotechnology Cat#sc-1688, RRID:AB_627576. The protein was detected, as expected, in the cytosol and the focal adhesion sites of the cells, as reported in Fig. 1i.
Rabbit monoclonal Anti-RAS (27H5) (WB: 1/1000) Cell Signaling Technology, Cat#3339 RRID:AB_2269641. The antibody was validated in this manuscript by Western blot in mouse cells and with RAS activity assay in mouse tissue, after administration of Cre recombinase and subsequent induction of KrasG12D expression (Reported in Fig. 2e and Fig. 7b respectively).
Purified Mouse Anti-p21 (SX118) (WB, 1:1000) BD Pharmingen Cat#556430, RRID:AB_396414. The antibody was validated in this manuscript by Western blot in mouse cells, after transduction with a Cre-expressing lentiviral construct to knockout p53 (Reported in Fig. 2e).
Mouse monoclonal Anti-FLAG® (M5) (WB, 1:5000), Sigma-Aldrich Cat#F4042, RRID:AB_439686. The antibody was validated in this manuscript by Western blot in human and mouse cells, after overexpression of Flag-tagged MCU (Reported in Extended Data Fig. 6c and Extended Data Fig. 7a).

Mouse monoclonal Anti-β-actin (AC-74) (WB, 1:2000) Sigma-Aldrich Cat#a-5316, RRID:AB_476743. The antibody was validated in human cells by Western blot by the manufacturer, showing a single specific band.
α-tubulin (WB, 1:2000) Sigma-Aldrich Cat#T6199, RRID:AB_477583. The antibody was validated in human cells by Western blot by the manufacturer, showing a single specific band.
Rabbit monoclonal Anti-Ki-67 (SP6) (IHC, 1:300) Thermo Scientific Cat#RM-9106, RRID:AB_2335745. Ki-67 had nuclear localization, as reported in the manufacturer's datasheet.
Mouse monoclonal Anti-pimonidazole (4.3.11.3) (IHC-F, 1:100) Hypoxyprobe™ Cat#HP6-200, RRID:AB_2801307: (Hofer, Mitchell et al. 2005).

Eukaryotic cell lines

Policy information about cell lines

Cell line source(s)	All human lung adenocarcinoma cell lines used in this study (A549, H358 and A427) were derived from male patients and were a kind gift from Dr. John Minna (UT Southwestern Medical Center, TX, USA) which is the original source of the NSCLC cell lines deposited in ATCC. HEK293T cells were obtained from ATCC (CRL-11268). We generated the MEFs and genotyped for provenance. The MEFs were generated in this study as described in the materials and methods.
Authentication	All cell lines were DNA fingerprinted for provenance.
Mycoplasma contamination	All cell lines tested negative for mycoplasma.
Commonly misidentified lines (See ICLAC register)	None of the cell lines used in the study belongs to commonly misidentified cell lines according to the ISLAC register.

Animals and other organisms

Policy information about studies involving animals; ARRIVE guidelines recommended for reporting animal research

Laboratory animals	Mice were maintained under a temperature of 21°C +/- 2°C, humidity 50% +/- 10% with a standard 12hr light/dark cycle and were fed ad libitum. Only male mice littermates were used for the tumor burden/number-related experiments. The mixed background Cre-inducible LSL-KrasG12D/WT;p53flox/flox;Plcγ1flox/flox mouse model was obtained by back-crossing for eight generations the B6.129SS4-krastm4Tyj/J x B6.129P2-Trp53tm1Brn/J and B6(Cg)-Plcg1tm1Flh/J strains. Tumor formation was induced at 8 weeks of age and mice were sacrificed 10 weeks later. For the xenotransplantation studies in vivo, cells were injected subcutaneously to male NOD.Cg-Prkdcscid Il2rgtm1Wjl/SzJ (NSG) mice at 6-8 weeks of age. The mice were closely monitored on a daily basis and the size of the tumors was measured with a caliper every 2-3 days. Mice were sacrificed when the tumor volume reached 1000mm3.
Wild animals	The study did not involve wild animals.
Field-collected samples	The study did not involve samples collected from the field.
Ethics oversight	Animal handling and experimental procedures were performed in compliance with the federal guidelines and were approved by the cantonal veterinary commission and animal welfare officer (AWO) of the Veterinaerdienst de Kantons Bern.

Note that full information on the approval of the study protocol must also be provided in the manuscript.

Human research participants

Policy information about studies involving human research participants

Population characteristics	The tissue microarray (TMA) contains lung cancer tissue from 199 human patients diagnosed with lung cancer (specifically with lung adenocarcinomas). The tissue derived from resection specimens of patients treated with curative surgery consecutively diagnosed between 1988 and 2008 at the Institutes of Pathology at the University Bern and University Hospital Basel. All NSCLC were reviewed for histology according to the current 2015 WHO recommendations (Reference: Travis W, Brambilla E, Burke A, Marx A, Nicholson A (2015) WHO classification of tumours of the lung, pleura, thymus and heart, 4th edn. IARC Press, Lyon.) The TMA was constructed from consecutive resection lung adenocarcinoma specimens with an adequate amount of FFPE tumor tissue for TMA construction. TMA construction was performed as previously described from paraffin-embedded (FFPE) tumor tissues fixed in 10% neutral buffered formalin with a punch diameter of 0.6 mm (Reference: PMID: 24853178 and PMID: 11568893). Patient's clinico-pathological and follow-up data were collected from hospital charts and questionnaires sent to the primary care physicians. No separation of patients according to sex, age or mutational status (i.e. KRAS mutation status) was applied in this study. The information on sex and age of all patients is included in Supplementary Table 2.
Recruitment	Early stage lung cancer (lung adenocarcinomas) from patients undergoing initial surgical resection without prior therapeutic treatment consecutively diagnosed between 1988 and 2008 at the Institutes of Pathology, University Bern and University Hospital Basel. No self-selection bias or other biases were present. The patients` tumor tissue was not screened for any genetic alterations.
Ethics oversight	The use of human samples and retrospective data was approved by the Swiss Association of Research Ethics Committees (Swissethics), institute: Kantonal Ethikkommission for research. All samples were provided upon patients consent. The study is compliant with all relevant ethical regulations regarding research involving human participants.

Note that full information on the approval of the study protocol must also be provided in the manuscript.

Flow Cytometry

Plots

Confirm that:

☒ The axis labels state the marker and fluorochrome used (e.g. CD4-FITC).

☒ The axis scales are clearly visible. Include numbers along axes only for bottom left plot of group (a 'group' is an analysis of identical markers).

☒ All plots are contour plots with outliers or pseudocolor plots.

☒ A numerical value for number of cells or percentage (with statistics) is provided.

Methodology

Sample preparation	To measure ROS levels, 1 x 106 cells were resuspended in 1µM Dihydrorhodamine 123 (DHR) (Sigma-Aldrich, D1054) in PBS and incubated for 30 min at 37oC. For LD measurement, 1 x 106 cells were gently washed with PBS and fixed with 4% paraformaldehyde for 10 min at room temperature. After removing the fixative solution, cells were washed 2 times with PBS to remove residual paraformaldehyde and stained with 1X LipidTOX Deep Red Neutral Lipid Stain solution (Invitrogen, H34477) for 30 min. The cells were then washed with PBS, before performing the assay as previously described. For the Annexin V/PI cell death assay, cells were plated at low confluency in a 12-well plate and treated as described in the figure legends. On the day of the assay, cells were washed with staining buffer (150mM NaCl, 4mM KCl, 2.5mM CaCl2, 1mM MgSO4, 15mM HEPES pH 7.2, 2% FBS and 10mM NaN3) and stained with Atto633-conjugated Annexin V for 20 min in the dark, on ice. Cells were then washed with staining buffer and resuspended in 200µL Propidium Iodide (PI) at a final concentration of 2µg/mL (MEFs), or 40µg/mL (A549). To inhibit caspase-induced cell death, cells were treated with 20 µM Q-VD-OPH 18h before staining.
Instrument	Flow cytometry was performed with a BD FACSLyric instrument.
Software	Data were analysed using the FlowJo V10 workspace.
Cell population abundance	The comparison between control and experimental condition was performed by considering the shift in geometric mean of the signal peak for each fluorophore.
Gating strategy	For every flow cytometry analysis, cells were gated according to their forward and side scatter values, in order to exclude cell clusters and debris. Please refer to Supplementary Fig. 1 for the gating strategy.

☒ Tick this box to confirm that a figure exemplifying the gating strategy is provided in the Supplementary Information.